Photoluminescence of Er^{3+}-implanted amorphous hydrogenated silicon suboxides

A. Janotta,* M. Schmidt, R. Janssen, and M. Stutzmann
Walter Schottky Institut, Technische Universität München, Am Coulombwall 3, 85748 Garching, Germany

Ch. Buchal
Forschungszentrum Jülich, Institut für Schichten und Grenzflächen (ISG-IT), 52425 Jülich, Germany
(Received 13 December 2002; revised manuscript received 13 May 2003; published 28 October 2003)

Erbium ions incorporated into amorphous hydrogenated silicon suboxides (a-SiO_x:H) allow to overcome the disadvantages of Er^{3+} in c-Si such as the limited solubility, the strong quenching of the luminescence at room temperature, and the need for co-doping with electronegative atoms. a-SiO_x:H alloys have an enhanced Er solubility and easily variable oxygen content, thereby providing favorable atomic environments for an efficient Er luminescence and reduced excitation backtransfer due to deeper localized band-tail states. In the present study, Er^{3+} doses up to 7×10^{14} cm^{-2} were implanted into a-SiO_x:H with oxygen content between 0 and 44 at. %. Optical properties such as the absorption coefficients and the photoluminescence (PL) spectra of the Er^{3+} ions and of the SiO_x host were investigated as a function of erbium implantation dose, oxygen content, defect density, temperature, and annealing treatment. It was found that annealing is a requirement for activating the characteristic Er PL at 1.54 μm mainly due to a reduction of implantation induced defects. The intensity of both the intrinsic SiO_x and the Er PL was found to be inversely proportional to the defect density as measured by electron spin resonance or subgap absorption. The Er PL is additionally enhanced upon annealing, probably as a result of better structural arrangements of the Er ions. The Er PL intensity increases approximately linearly with the implantation dose. An increase of the oxygen content (and correspondingly of the optical band gap) of a-SiO_x:H causes no drastic changes in the erbium luminescence energy and intensity, whereas the intrinsic PL shifts to higher photon energies according to the larger band gap. Already low O concentrations of a few percent provide favorable Er environments. The main advantage of a-SiO_x:H as a host matrix is revealed by temperature-dependent PL measurements. For high oxygen contents, the thermal quenching of both the Er^{3+} and the intrinsic PL is strongly reduced. In an a-SiO_x sample with 44 at. % oxygen, the Er PL is only quenched by 20% between 77 and 300 K. In contrast, the quenching of the intrinsic PL for all [O] is roughly one order of magnitude stronger than that of the Er PL. These PL measurements were complemented by PL excitation experiments over a wide spectral range. We have observed that the Er^{3+} PL is excited about one order of magnitude more efficiently when pumped with sub-band-gap light compared to band-to-band excitation. The experimental results are discussed with regard to the two currently proposed Er^{3+} excitation models, the defect-related Auger effect and the Förster transfer mechanism.

DOI: 10.1103/PhysRevB.68.165207 PACS number(s): 61.43.Dq, 61.72.Tt, 71.20.Eh, 78.40.Pg

I. INTRODUCTION

Rare-earth erbium ions possess an incompletely filled $4f$ shell that is screened by the $5s$ and $5p$ shells. In its $3+$ charge state, it exhibits a luminescence at approximately 1.54 μm, the transmission maximum of conventional silica-based optical fibers. This fact has made Er^{3+} an interesting candidate for the incorporation into silicon-based semiconductor materials. Owing to the screening mentioned above, the luminescence energy is rather insensitive to the chemical nature of the host matrix. The photoluminescence (PL) originates from internal transitions of the excited $^4I_{13/2}$ state to the ground state $^4I_{15/2}$ of the $4f$ shell. It usually consists of many lines centered around 1.54 μm that are caused by the crystal-field splitting of the $4f$ levels. Owing to the disordered surrounding in amorphous hosts, the luminescence—in contrast to crystalline silicon[1] (c-Si)—is rather featureless, with only the two main transitions at 1550 and 1538 nm remaining discernable. In the case of isolated ions, the $^4I_{13/2}\rightarrow{}^4I_{15/2}$ transition is dipole forbidden. It was found that it becomes partially allowed by co-doping with impurities such as oxygen, carbon, fluorine, or nitrogen.[2–4] The strong electronegativity of these co-dopants induces strong local fields with low symmetry around the Er^{3+} ions and thus admixes other orbital momentum states to the f wave function so that the selection rules are relaxed, the radiative recombination lifetimes are reduced, and the erbium PL intensity is significantly enhanced.

Photoluminescence and electroluminescence of Er in crystalline silicon co-doped with oxygen have been demonstrated even at room temperature.[2–7] However, the incorporation of Er^{3+} into c-Si has certain drawbacks such as the limited solubility ($\approx10^{19}$ cm^{-3}), the low efficiency of the room-temperature luminescence due to thermal quenching, and the need for co-doping with oxygen or carbon. Using amorphous materials such as amorphous silicon[8–10] (a-Si:H) and amorphous hydrogenated silicon suboxides[11] (a-SiO_x:H) or also partially crystallized silicon oxides[12] semi-insulating polycrystalline silicon (SIPOS) as a host for erbium can help to reduce these problems. Er concentrations above 10^{20} cm^{-3} can easily be incorporated due to the flexibility of the amorphous network. Furthermore, the presence of large fractions of electronegative oxygen in a-SiO_x:H (even a-Si:H already contains residual oxygen in the range

of some 100 ppm) provides the desired strong local crystal field with low symmetry, which enhances the PL by making the $^4I_{13/2} \rightarrow {}^4I_{15/2}$ transition partially allowed. Additionally, the optical gap of silicon suboxides can easily be tuned by varying the oxygen content.[11] Thus, it should be possible to obtain optimal conditions for an efficient energy transfer from the host matrix to the luminescent Er ions—even at room temperature. The larger band gaps of a-SiO_x:H compared to a-Si:H or c-Si and the correspondingly deeper localized states also help to reduce strong thermal quenching. Finally, doping of SiO_x:H is possible so that light-emitting p-i-n diodes containing erbium can be fabricated in principle.[11,13]

The aim of this work is to study in detail the excitation mechanism of erbium ions in disordered silicon-oxygen systems. It is of particular interest to elucidate the energy transfer between the host matrix and Er^{3+} as a function of the optical band gap and of the oxygen environment. Also, the importance of structural defects for the excitation of the rare-earth ions and for competitive radiative or nonradiative channels is an issue that requires thorough investigation. We report the results of a systematic study of Er^{3+} in a-SiO_x:H with oxygen contents between 0 and 44 at. %. Particular attention has been paid to a comparison of the extrinsic Er^{3+} and the intrinsic a-SiO_x luminescence as a function of the oxygen content, defect density, temperature, and excitation energy.

The results presented in this paper are expected also to be of relevance for Er^{3+} in the vicinity of silicon-oxygen interfaces in general. Disordered substoichiometric Si-O phases are very likely to be present in materials such as SIPOS (Ref. 12) or in matrices containing Si nanocrystals[14–17] as well.

II. EXPERIMENT

Amorphous hydrogenated silicon suboxides were deposited by plasma-enhanced chemical vapor deposition (PECVD) from the source gases SiH_4, H_2, and CO_2. By varying the SiH_4/CO_2 gas flow ratio, oxygen concentrations between 0 and 50 at. % can be achieved. This leads to optical gaps between 1.9 and 3.0 eV (E_{04}, the energy where the absorption coefficient reaches 10^4 cm^{-1}), which makes SiO_x a favorable material for applications in silicon-based optoelectronics. The intrinsic SiO_x thin films (500–1000 nm) were deposited on Corning 7059 glass at 250 °C. The oxygen contents were varied between 0 and 44 at. % and were determined by energy-dispersive x-ray spectroscopy (EDX), which was calibrated by quantitative elastic recoil detection (ERD) analysis. All oxygen concentrations given in the text refer to the atomic ratio $[O]/([O]+[Si])$.

Erbium doses ranging from 4.5×10^{12} to 7×10^{14} cm^{-2} were implanted at the Forschungszentrum Jülich, resulting in erbium peak concentrations between 10^{18} and 10^{20} cm^{-3} (Table I). Three single implantations at an ion energy of 200 keV and one multiple-energy implantation at 100, 200, and 400 keV were performed. The latter lead to a more homogeneous distribution of the Er ions within the first 200 nm of the SiO_x film, which was confirmed by TRIM code simulations [''transport of ions in matter'' (Ref. 18)] at the Forschungszentrum Jülich. The single implants resulted in Gaussian-shaped distributions at penetration depths of roughly 100 nm and with a full width at half maximum of about 50–60 nm. The implantations were performed on SiO_x films with oxygen contents from 0 to 44 at. %. Details can be seen in Table I. Annealing in N_2 atmosphere for 1 h at temperatures between 100 and 450 °C was used to reverse the unwanted damaging effects of implantation, to passivate dangling-bond defects, to study the effects of hydrogen outdiffusion, and to investigate the corresponding behavior of the Er and SiO_x PL. Photothermal deflection spectroscopy[19] (PDS) and optical transmission measurements were used to determine the absorption coefficient α and the optical gap E_{04}.

TABLE I. Compilation of the different Er implantation doses at the respective ion energies, the total implantation doses, the Er peak concentrations, and the oxygen contents of a-SiO_x films investigated.

Er^{3+} implantation dose (cm^{-2})	Ion energy (keV)	Total Er^{3+} dose (cm^{-2})	Maximum Er^{3+} concentration (cm^{-3})	Oxygen content (at. %)
4.5×10^{12}	200	4.5×10^{12}	10^{18}	30, 40
4.5×10^{13}	200	4.5×10^{13}	10^{19}	30, 40
4.5×10^{14}	200	4.5×10^{14}	10^{20}	30, 40
1.5×10^{14}	100			
$+2.0\times10^{14}$	200			
$+3.5\times10^{14}$	400	7×10^{14}	7×10^{19}	0–44

The PL was excited by an argon-ion laser at wavelengths between 458 and 514 nm, a He-Ne laser at 632 nm and a titanium sapphire laser at $\lambda_{exc}=920-995$ nm. The laser beam was coupled into a glass fiber and directed onto the samples mounted in a liquid-nitrogen ($T=77$ K) or a liquid-helium cryostat ($T=4-300$ K). For PL detection, an Oriel $\frac{1}{4}$-m monochromator combined with a Si avalanche diode (1.2–2.0 eV) or a Ge detector (0.7–2.0 eV, cooled with liquid nitrogen) was used. All PL spectra were corrected for the sample absorption at the excitation wavelength and for the spectral response of the detection setup.

III. RESULTS

A. Defect absorption

Implantation of erbium ions causes significant damage in the a-SiO_x:H layers. These structural changes can be monitored by measuring the sub-band-gap absorption coefficient of the samples. From characteristic parameters such as the optical gap E_{04}, the Urbach energy E_0 (the band-tail ''steepness'' as a measure of the disorder in the material), and the dangling-bond density (derived from the defect absorption at photon energies between 1.0 and 1.7 eV), differences between and changes of samples subjected to different types of treatments can be quantified and compared. It should be pointed out that in this study we are not only dealing with the damages after implantation and with the effect of different Er doses at different ion energies (leading to different penetra-

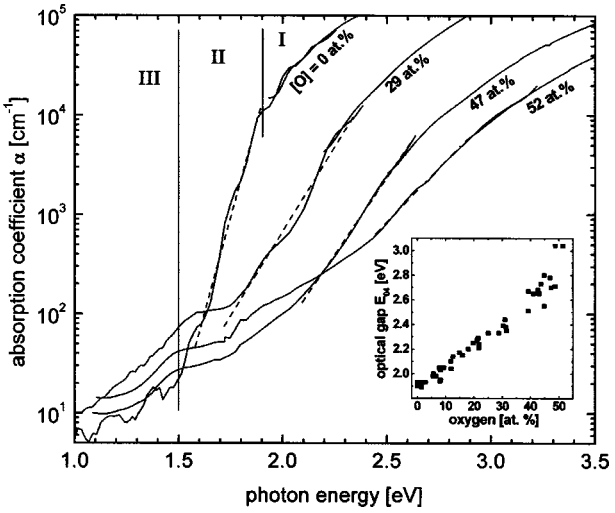

FIG. 1. Absorption spectra of as-deposited, intrinsic, unimplanted a-SiO_x:H with different oxygen contents of 0, 29, 47, and 52 at. %. The spectral regions of band-to-band (I), band-tail (II), and defect absorption (III) are indicated for the sample without oxygen (a-Si:H). Straight dashed lines are fits to the band tails to determine the Urbach energy. The inset shows the dependence of the band gap on the oxygen content.

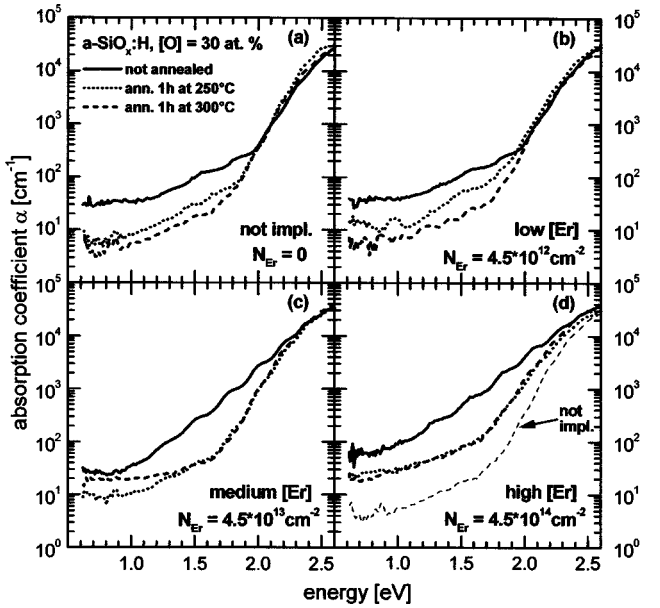

FIG. 2. Absorption spectra of SiO_x with 30 at. % oxygen after Er implantation (solid lines) and after successive annealing for 1 h at 250 °C (dotted lines) and 300 °C (dashed lines). (a) Without Er implantation; (b) low Er dose, $N_{Er}=4.5\times10^{12}$ cm^{-2}; (c) medium Er dose, $N_{Er}=4.5\times10^{13}$ cm^{-2}; (d) high Er dose, $N_{Er}=4.5\times10^{14}$ cm^{-2}.

tion depths), we also have to take into account that the SiO_x thin films themselves possess quite different defect properties at different oxygen contents. Furthermore, all these samples—as deposited and implanted—were subjected to different annealing procedures, which again alter the structural properties observed by absorption measurements. These measurements do not only provide information about the material properties such as band gap, Urbach energy, or defect density, but also allow us to correct the PL spectra for the influence of the different sample properties, so that absolute comparisons become possible.

Figure 1 displays the sub-band-gap absorption spectra for a set of as-deposited, unimplanted silicon suboxides with oxygen concentrations of 0, 29, 47, and 52 at. %. For the curve of the a-Si:H sample (0 at. % [O]) the three different regions of absorption in amorphous semiconductors are indicated. Region I corresponds to band-to-band absorption, region II originates from absorption processes involving band-tail states, and region III arises from absorption via dangling-bond defect states in the middle of the forbidden gap ($g\approx2.0055$, as known from ESR measurements). These regions are also discernible for the other curves, however, but become less distinguishable with increasing oxygen concentration. The value of the band gap E_{04} increases from approximately 1.9 to 3.0 eV for [O] between 0 and 50 at. %. This is shown in more detail in the inset of Fig. 1. Here, the slow linear increase of E_{04} up to roughly 45 at. % corresponds to oxygen contents where the conduction (CB) and valence (VB) bands are still dominated by Si-Si bonds, whereas above 45 at. % oxygen these Si-Si bonds are gradually replaced by oxygen lone pairs (VB) and Si-O bonds, causing a more rapid increase of the band gap.[20,21] The band tails (region II) of our SiO_x samples start out with an Urbach energy of about 70 meV for a-Si:H (nonoptimized), broaden significantly with increasing oxygen content and reach a value of roughly 200 meV for 50 at. % oxygen. Thus, the presence of oxygen alone increases the disorder in the amorphous films. Also the defect absorption changes with increasing oxygen content. In the energy region between 1.0 and 1.5 eV, the sample without oxygen possesses the lowest defect absorption. Introducing oxygen creates defects and accordingly increases α. Defect densities can be calculated from sub-band-gap absorption using a calibration procedure described elsewhere.[11,22] However, this calibration is not trivial because with increasing oxygen content the optical gap and also the region of defect absorption shift in energy. Therefore, the uncertainty in the deduced absolute defect concentrations N_D is approximately a factor of 2, whereas the relative errors between samples are much smaller.

The influence of different Er^{3+} implantation doses and subsequent annealing steps on the absorption spectra is displayed in Fig. 2 for an a-SiO_x:H sample with [O] $=30$ at. %. Figure 2(a) shows the unimplanted sample. The optical gap E_{04} is between 2.3 and 2.4 eV, the Urbach energy E_0 is about 100 meV, and the as-deposited defect density is in the range of $N_D\approx10^{18}$ cm^{-3}. Annealing at 250 and 300 °C slightly reduces E_{04} and the Urbach energy E_0. However, the sub-band-gap defect absorption decreases by almost one order of magnitude ($N_D\approx10^{17}$ cm^{-3}). Implantation with a low erbium dose [$N_{Er}=4.5\times10^{12}$ cm^{-2}, Fig. 2(b)] produces few damaging effects in the spectra at all annealing steps in comparison with the unimplanted sample. Unfortunately, Er doses below 10^{13} cm^{-2} turned out to be insufficient to obtain any luminescence from the rare-earth ions. In contrast, medium and high Er doses [Figs. 2(c) and 2(d)] cause significant damage in the material. The band tails

are broadened considerably in both cases, resulting in Urbach energies above 200 meV. The band gap itself is unaffected, except for superimposed damage-induced band-tail states. Also, the dangling-bond absorption between 1.0 and 1.6 eV is increased by almost one order of magnitude ($N_D \approx 10^{19}$ cm^{-3}). Annealing enables a relaxation of disorder in the material and a reconstruction of dangling bonds. Thus, the band tails steepen again and the Urbach energies are reduced to 120 and 140 meV for medium and high Er doses, respectively. The defect density is lowered by approximately half an order of magnitude upon annealing, but especially for high erbium fluences the unwanted damaging effects of implantation cannot be reversed completely, even for annealing at 300 °C. The Urbach tails are still broader (140 vs 100 meV) and the dangling-bond density is still more than half an order of magnitude higher than that of the unimplanted annealed sample [thin dashed line in Fig. 2(d)]. Quite similar results with regard to implantation damage and annealing were obtained for the implantation of different ions (Si^+, Ge^+, H^+, B^+, P^+, Ar^+, Xe^+, etc.) with energies up to 1 MeV into *a*-Si, *a*-Si:H, and *a*-SiN_x:H.[23–26] From such absorption measurements, no statement can be made about the incorporation and microscopic environment of Er in *a*-SiO_x:H. No direct absorption of Er ions is visible in the absorption spectra even for the highest implantation doses. In glass fibers where Er^{3+} is completely surrounded by oxygen (forming Er_2O_3 complexes), the absorption cross section is only in the range of 10^{-21} cm^2.[27] This value can also be regarded as an upper limit for Er in SiO_x. Therefore, even for Er concentrations up to 1 at. %, resonant Er absorption would be too weak to be seen above the background of defect absorption in *a*-Si:H (Ref. 28) or *a*-SiO_x:H. Note that the small absorption peak at 0.85 eV, which can be recognized in some of the PDS spectra, arises from the second harmonic of the O-H vibration of the glass substrate and not from Er or SiO_x.[29–31]

Figures 3(a)–3(c) summarize the effect of Er^{3+} implantation on silicon suboxides with varying oxygen content. A multiple-energy erbium implantation with a total dose of 7×10^{14} cm^{-2} was performed on *a*-SiO_x:H with oxygen content from 0 to 44 at. %. After implantation annealing was performed for 1 h at 275 °C under nitrogen atmosphere. This is an annealing temperature sufficiently high to reverse most of the damage by Er-ion bombardment, but still low enough to prevent the out-diffusion of hydrogen above 300 °C, which is known to deterioriate the structural quality. Shown in Fig. 3 are the optical gap E_{04}, the Urbach energy E_0, and the defect absorption as a function of the oxygen concentration. For each oxygen concentration the corresponding data of an as-deposited sample before implantation (comparable to Fig. 1), directly after implantation and after implantation and annealing are plotted. Implantation reduces the value of E_{04} by approximately 0.2 eV. As already mentioned, this is not due to a real reduction of the band gap, but rather due to the additional absorption of damage-induced band-tail states extending to $\alpha \approx 10^4$ cm^{-1} on the absorption curves. This apparent shift disappears completely after annealing, which removes the additional band-tail states. The Urbach energies [Fig. 3(b)], which for as-deposited samples vary from 70 to

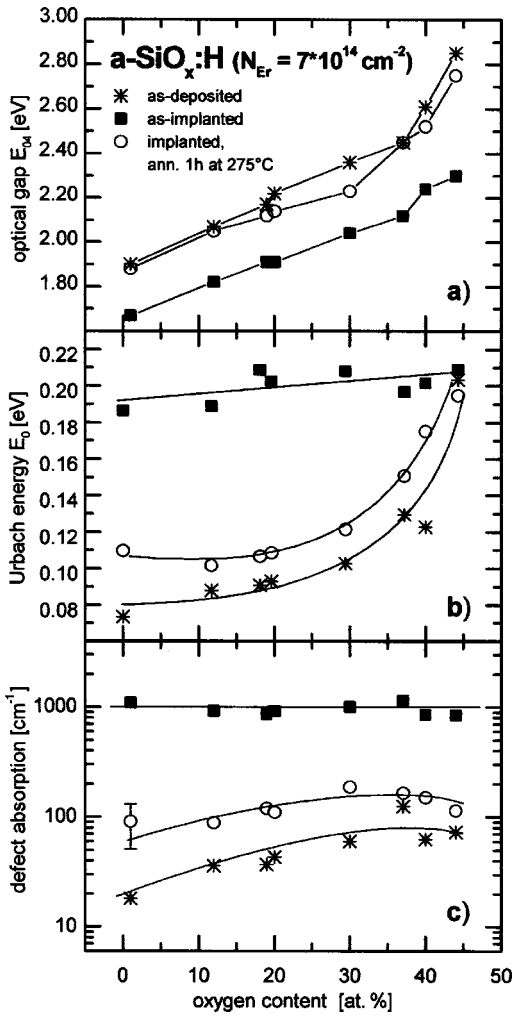

FIG. 3. (a) Optical gap E_{04}, (b) Urbach energy E_0, and (c) defect absorption coefficient of *a*-SiO_x:H as a function of oxygen content ($N_{Er} = 7 \times 10^{14}$ cm^{-2}). Each graph shows the data for the samples in the as-deposited, unimplanted state (asterisks), the as-implanted state (solid squares), and after implantation and annealing for 1 h at 275 °C (open circles). The lines are guides to the eye.

200 meV as a function of oxygen content, increase drastically after implantation. The Urbach energy of all implanted samples is around 200 meV, irrespective of the oxygen content. This confirms that the same high Er dose introduces the same amount of disorder in all SiO_x samples that are still characterized by a percolating Si-Si backbone structure. After annealing, the Urbach energies decrease again and the original dependence of E_0 on the oxygen content reappears, although the low values of the unimplanted samples can not be entirely recovered. The deep defect absorption is difficult to extract for the implanted, unannealed samples because of spectral overlap with the implantation-induced tail states. Therefore, only the defect absorption coefficient at a characteristic energy is plotted in Fig. 3(c). (This characteristic energy increases from 1.3 eV for [O]=0 to 1.7 eV for [O] =50 at. %; see Refs. 11 and 22 for details.) This figure confirms the overall trend that the defect density, which is increased by roughly one order of magnitude after implantation, can be partly annealed out again. This beneficial effect

of annealing is, however, less pronounced for SiO_x with higher oxygen content, which already contains more defects and disorder.

B. Photoluminescence

In the following, the PL of the Er^{3+} ions as well as that of the a-SiO_x:H host material will be discussed as a function of erbium dose, annealing, oxygen content, temperature, and excitation energy. Using the measured absorption coefficients and the calculated Er depth profiles, all PL spectra and intensities presented below were normalized to the number of absorbed photons and corrected for the fact that the Er implantation affects only the optical and luminescence properties of the first 100–200 nm of the SiO_x layers.

1. Dependence on Er implantation dose and defect annealing

Particularly after heavy implantation, hardly any PL either from the SiO_x host or from the rare-earth ions can be detected. Annealing of the induced structural damage turned out to be crucial to activate both kinds of luminescence, a fact that correlates well with partial removal of the implantation-induced defects by annealing, already observed in the absorption spectra (Fig. 2). Figure 4(a) shows spectra of a heavily implanted a-SiO_x:H sample ($[O] \approx 30$ at. %, $E_{04} \approx 2.3$ eV, $N_{Er} = 4.5 \times 10^{14}$ cm^{-2}, $T = 77$ K), where both extrinsic and intrinsic PL maxima can be seen. The intrinsic PL is situated at roughly 1.4 eV with a spectral width of about 400 meV. There is hardly any luminescence in the as-implanted state, but PL appears after a first annealing step at 250 °C for 1 h and increases further after a second step at 300 °C. The shoulders, which can be seen in some of the intrinsic SiO_x spectra, are due to thin-film interference. The narrow erbium luminescence at 0.8 eV on the left side of Fig. 4(a) is shown on a larger scale in Fig. 4(b). The two main Er PL lines at 1538 and 1550 nm arising from $^4I_{13/2} \rightarrow {}^4I_{15/2}$ transitions can be resolved. Similar to the intrinsic luminescence, the Er PL is completely absent in the as-implanted state, but increases with successive annealing. Thus, defect annealing is a requirement for activating and detecting erbium PL in a-SiO_x. Comparable behavior was found in Er-implanted and Er-cosputtered a-Si:H (Refs. 10 and 32) with low oxygen content (≤ 1 at. %). Therefore, most of the following spectra and data were measured for samples that had been annealed at optimum conditions (1 h at 250–300 °C). The systematic determination of these optimum conditions will be discussed in more detail in conjunction with Fig. 6 below.

The dependence of the intrinsic and the Er photoluminescence at 77 K on the Er dose is shown in Fig. 5, again for an oxygen content of 30 at. %. Annealing was performed at 300 °C for 1 h. The displayed spectra were obtained from one unimplanted sample and from four samples with different Er implantation doses between 4.5×10^{12} and 7×10^{14} cm^{-2}. The intensity of the erbium PL [Fig. 5(a)] increases monotonically with the implanted amount of Er. Doses larger than 10^{13} cm^{-2}, corresponding to peak concentrations of 10^{19} cm^{-3}, are necessary for the detection of an effective PL. A similar critical Er concentration between 10^{18} and 10^{19} cm^{-3} was found by Kühne *et al.*[28] These authors suggested that in a dipole-mediated Förster energy transfer process the distances to the Er ions would be too large (>100 Å) for an efficient PL excitation at low Er concentrations. Fortunately, the solubility of erbium in SiO_x exceeds 10^{20} cm^{-3} and is in the range of some tenths of atomic %. In contrast to the Er PL, the intensity of the intrinsic SiO_x PL decreases for samples implanted with increasing Er dose [Fig. 5(b)]. This likely occurs due to a more persistant defect density that cannot be eliminated completely by annealing and that favors nonradiative recombination. Thus, the intrinsic PL intensity in Fig. 5(b) decreases by approximately a factor of 4 upon Er implantation with the highest dose, in agreement with the corresponding increase of the defect absorption shown in Fig. 2(d). Also, the intrinsic PL peak position is shifted from about 1.4 to 1.3 eV for higher Er doses due to the band-tail broadening and the resulting band-gap narrowing.

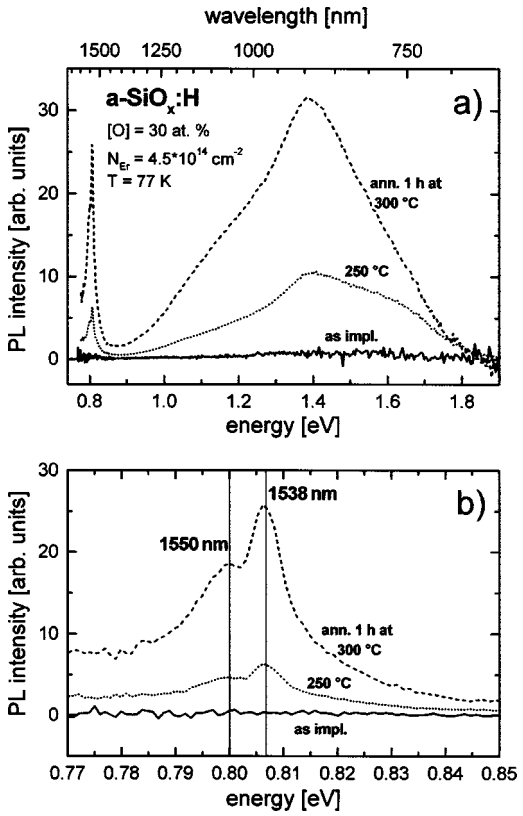

FIG. 4. SiO_x and Er^{3+} PL at 77 K of an a-SiO_x:H sample ($[O] \approx 30$ at. %, $E_{04} \approx 2.3$ eV) implanted with high Er dose (4.5×10^{14} cm^{-2}) as a function of annealing (as implanted, solid line; annealed 1 h at 250 °C, dotted line; annealed 1 h at 300 °C, dashed line). (a) Er and a-SiO_x PL. (b) Enlarged view of the Er^{3+} PL with the two characteristic lines at 1538 and 1550 nm.

However, from these general observations it is still not possible to quantitatively distinguish various contributions to the enhancement and quenching of the Er^{3+} and the SiO_x PL as a function of implantation dose and annealing. For example, the Er PL could increase with annealing due to a reduction of implantation-induced defects and disorder and thus a more effective energy transfer to the erbium ions.[10] On

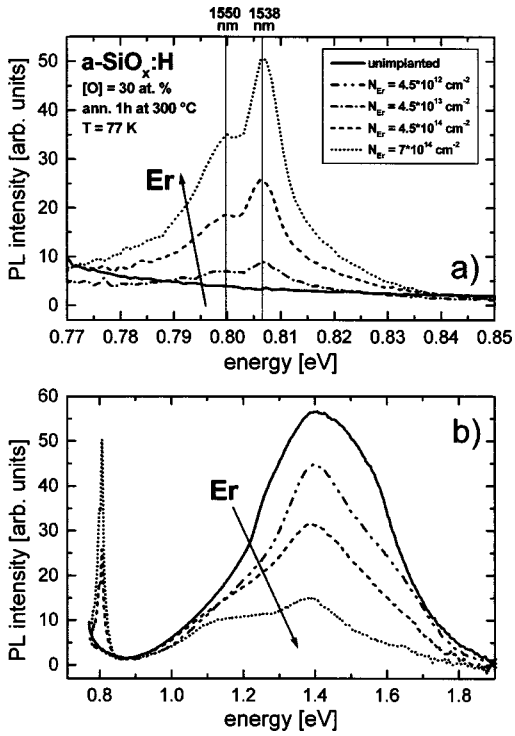

FIG. 5. Intrinsic and Er^{3+} PL at 77 K for a-SiO_x:H (annealed at 300 K for 1 h) with 30 at. % oxygen and an optical gap $E_{04} \approx 2.3$ eV as a function of Er implantation dose. (a) Detailed view of the Er^{3+} PL. The lines drawn indicate the two characteristic Er^{3+} lines at 1538 and 1550 nm. (b) SiO_x and Er PL.

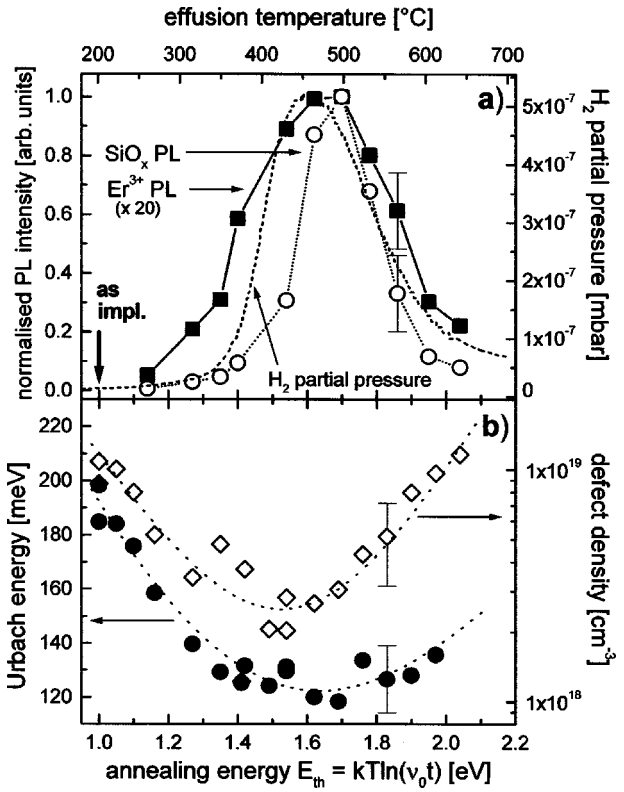

FIG. 6. (a) Normalized SiO_x (open circles) and Er^{3+} PL (solid squares)—both at 77 K—and hydrogen partial pressure (dashed line) during thermal effusion. (b) Urbach energy (solid circles) and defect density (open diamonds) from the absorption spectra as a function of annealing energy and effusion temperature. The sample studied contained roughly 30 at. % oxygen ($E_{04} \approx 2.3$ eV) and was implanted at an Er fluence of 4.5×10^{14} cm^{-2}. The dotted lines are guides to the eye. The relative uncertainties of the respective quantities are shown exemplarily by an error bar on one of the data points of each data set.

the other hand, also the formation of a more favorable Er environment upon annealing or a different incorporation with increasing Er doses might contribute to this effect.[10,33] As far as the intrinsic SiO_x PL is concerned, a nonradiative quenching approximately proportional to the density of (existing and implantation-induced) dangling bonds is suggested by the data in Figs. 2 and 5. However, in addition a competitive energy-transfer mechanism between the intrinsic PL and the Er PL might contribute to the decrease of the intrinsic SiO_x PL with higher Er contents.[28]

In order to shed more light on this general question, we have investigated the behavior of both photoluminescence signals and of relevant structural properties such as defect density and Urbach energy systematically as a function of annealing and Er dose. In Fig. 6, several relevant quantities of an a-SiO_x sample with 30 at. % oxygen and an Er dose of 4.5×10^{14} cm^{-2} are displayed as a function of effusion temperature (linear heating rate of $\beta = 20$ K/min) and of the corresponding characteristic annealing energy $E_{\mathrm{th}} = kT \ln(\nu_0 t)$ (calculated for isothermal annealing for $t = 1$ h and temperatures $T = 100-475\,^{\circ}$C). E_{th} is deduced from the rate of a thermally activated process and combines time and temperature, which allows us to compare isochronal and isothermal annealing procedures. The rate constant ν_0 in this relation was previously determined to $\nu_0 = 10^{10}$ s^{-1}.[11,34] As already shown in Fig. 4, the SiO_x as well as the Er^{3+} PL require an appropriate annealing for the activation of their luminescence [Fig. 6(a)]. Note that for $N_{\mathrm{Er}} = 4.5 \times 10^{14}$ cm^{-2} the integrated intrinsic PL at 77 K is roughly a factor of 20 larger than the Er PL. Starting from the as-implanted state at $E_{\mathrm{th}} \approx 1.0$ eV, both curves increase in a similar fashion by more than one order of magnitude upon annealing, show a peak around $E_{\mathrm{th}} \approx 1.6$ eV ($\approx$1 h at 300–325 °C) and decrease again towards higher annealing energies. Similar behavior was observed by Shin *et al.*[10] for Er-implanted a-Si:H. Upon closer inspection, however, one notices an earlier increase of the Er^{3+} PL at lower annealing energies, which will be discussed below. These findings can be compared to the annealing dependence of other quantities: Hydrogen is known to become mobile at annealing temperatures of about 250 °C, thus favoring a reduction of disorder by structural relaxation and the passivation of dangling bonds. This can be seen in Fig. 6(b) as an initial decrease of the defect density N_D from 10^{19} to 2×10^{18} cm^{-3} and of the Urbach energy E_0 from 200 to 120 meV. Upon further annealing, H begins to effuse from the samples as evidenced by a rise of the H partial pressure in effusion measurements [Fig. 6(a)]. From this point on the material quality deteriorates again, N_D starts to increase again, and the luminescence intensities are drastically reduced. A weaker deterioration is observed for the Urbach energy E_0, i.e., the amount of disorder remaining after im-

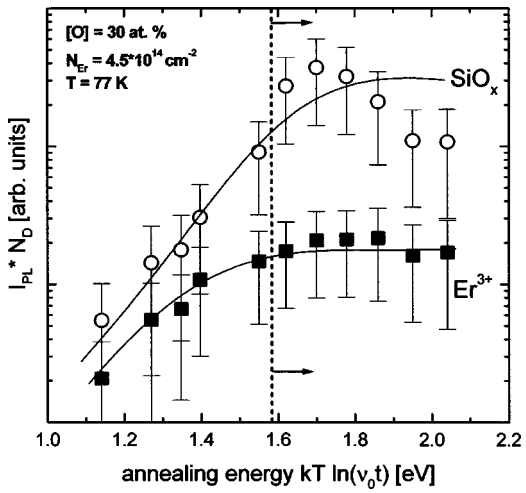

FIG. 7. Intensities of SiO_x and Er^{3+} PL at 77 K, multiplied with the respective defect densities N_D (obtained from sub-band-gap absorption in PDS spectra) as a function of the annealing energy. The SiO_x sample had 30 at. % oxygen and an optical gap of 2.3 eV. The Er^{3+} implantation dose was 4.5×10^{14} cm^{-2}. The lines are guides to the eye.

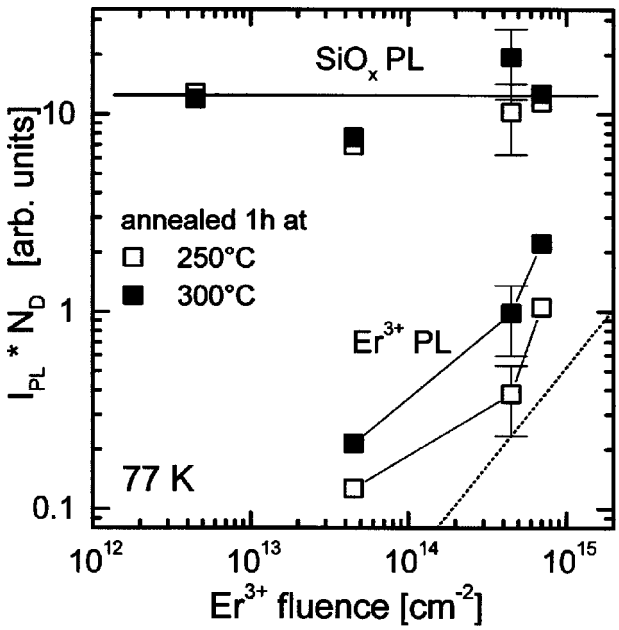

FIG. 8. Product of the intensities of SiO_x and Er^{3+} PL at two different annealing steps and of the respective defect densities N_D (obtained from sub-band-gap absorption in PDS spectra) as a function of Er implantation dose. The SiO_x samples had 30 at. % oxygen and an optical gap of 2.3 eV. The uncertainties of the $I_{PL}N_D$ products are shown by an error bar on one of the data points for each data set. The dotted line indicates a linear increase in this double-logarithmic plot. The other lines are guides to the eye.

plantation and annealing. An optimized annealing procedure can be deduced from Fig. 6 to consist of an isothermal annealing at about 300 °C for 1 h, which agrees very well with previous findings.[10,32,33] The principal limitation due to H out-diffusion at higher temperatures makes this a quite general value for amorphous Si alloys prepared by different techniques and containing various amounts of O and Er.

Upon closer inspection of Fig. 6(a), however, only the decaying edges of the two PL's and of the H_2 partial pressure overlap sufficiently well within the given uncertainties of the data. As for the rising edge, the Er PL increases distinctly earlier with respect to the hydrogen effusion and the SiO_x PL. Thus, in addition to the fact that the SiO_x and also the Er PL seem to be mainly affected by a competitive nonradiative recombination via midgap defects,[35] which leads to an approximately inverse dependence of both PL intensities on N_D, apparently additional mechanisms exist below the out-diffusion temperature of H_2 that have an enhancing effect on the Er PL.

In order to account for the influence of the defect density N_D on the PL intensity I_{PL}, the product of I_{PL} and N_D is plotted as a function of the annealing energy in Fig. 7. Above $E_{th}\approx1.6$ eV, this product $I_{PL}N_D$ of both the host and the rare-earth-ion PL is almost constant, which illustrates that dangling bonds, generated by hydrogen out-diffusion, are mainly responsible for the quenching of the PL in this annealing regime:

$$I_{PL}\propto 1/N_D \quad \text{for } E_{th}>1.6 \text{ eV}. \tag{1}$$

Below $E_{th}\approx1.6$ eV, in contrast, $I_{PL}N_D$ increases with successive annealing. This suggests the existence of non-defect-related mechanisms that enhance the luminescence intensity. For the SiO_x PL, the increase of $I_{PL}N_D$ below $E_{th}\approx1.6$ eV comprises almost two orders of magnitude. The reduction of the Urbach energy for annealing up to $E_{th}\approx1.6$ eV [Fig. 6(b)] seems to be responsible for this behavior: Steeper tails will allow a faster thermalization of geminate electron-hole pairs and, on the average, will result in a larger separation of thermalized photocarriers from nonradiative deep defects due to the reduced combined density of states. The $I_{PL}N_D$ product for Er^{3+}, on the other hand, increases by only one order of magnitude, but the absolute rise is faster [see Fig. 6(a)] and occurs at lower annealing energies. This gives rise to the assumption that the enhanced rare-earth-ion PL is due to Er^{3+} incorporation into a more favorable environment such as Er_2O_3 clusters or O-rich regions. Several studies have shown that the correct oxygen environment of erbium is crucial for an enhancement of its PL due to the corresponding noncentrosymmetric crystal field.[12,33,36–38] Annealing is known to additionally improve this oxygen coordination around Er.

In Fig. 8, the product $I_{PL}N_D$ at two different annealing steps is plotted as a function of erbium dose. For the intrinsic SiO_x PL, this product yields a constant value irrespective of the structural damage caused by the different implantation doses and irrespective of annealing at the two selected temperatures. The intensity of the Er^{3+} PL, when multiplied with N_D, shows the expected roughly linear increase with the amount of implanted ions at both annealing steps displayed:

$$I_{PL}(Er^{3+})\propto[Er]/N_D. \tag{2}$$

However, for annealing at 300 °C, the product $I_{PL}N_D$ of the Er luminescence is enhanced by roughly a factor of 2 com-

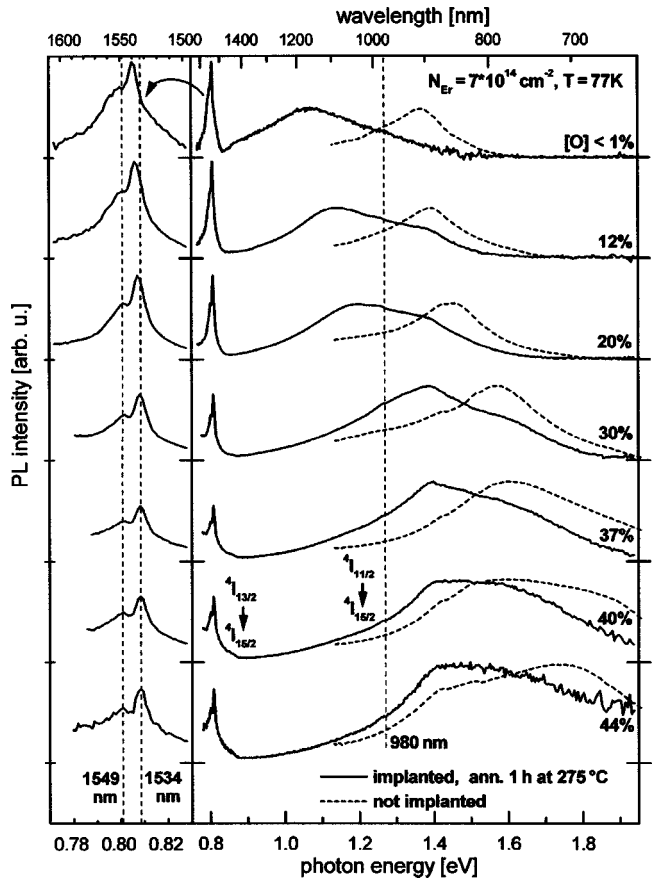

FIG. 9. Er^{3+} and SiO_x PL spectra at 77 K for oxygen contents between 0 and 44 at. %. The solid curves refer to samples that were multi-implanted with an Er dose of $N_{Er}=7\times10^{14}$ cm^{-2} and annealed afterwards at 275 °C for 1 h. The dashed SiO_x PL spectra are those of unimplanted, as-deposited samples with identical oxygen contents. The Er^{3+} luminescence is shown on a larger scale for all implanted samples on the left side of the diagram. The relevant erbium $4f$ transitions $^4I_{13/2}\rightarrow{}^4I_{15/2}$ and $^4I_{11/2}\rightarrow{}^4I_{15/2}$ are indicated by dashed straight lines.

pared to the 250 °C anneal for all Er doses, which is not the case for the intrinsic PL. This again leads to the conclusion that the Er^{3+} PL is not only increased due to defect annealing, but that it is also activated by the incorporation of erbium into a more favorable structural environment.

2. Influence of oxygen content and temperature

a-Si:H usually is subject to a residual oxygen contamination in the range of some tenths of atomic %.[9,10,37] This may already be helpful for the Er^{3+} luminescence because erbium ions can act as oxygen getters that only react with Si when the accessibility or the amount of O is limited.[36,37,39] The Er PL is further enhanced when the fraction of oxygen is increased above 1 at. %.[10,40,41] In the present study on silicon suboxides the range of oxygen contents was extended up to values of 44 at. %. Figure 9 shows the Er^{3+} and intrinsic PL at 77 K for oxygen concentrations between <1 and 44 at. %. Owing to the screening of the erbium ions by their $5s$ and $5p$ shells, the main peak of the Er PL remains rather constant at about 0.8 eV. Also, a small spectral feature due to the $^4I_{11/2}\rightarrow{}^4I_{15/2}$ transition from the second excited state to the Er^{3+} ground state can be recognized on top of all *a*-SiO_x:H(Er) PL spectra at 1.265 eV. This will be discussed in more detail later. A closer look at the better-resolved Er PL spectra in the left part of Fig. 9, however, reveals subtle changes of shape and position as a function of [O]. With increasing oxygen content, the two Er^{3+} peaks of the $^4I_{13/2}\rightarrow{}^4I_{15/2}$ transition tend to narrow and thus become better resolved. Additionally, their wavelengths shift from 1551 to 1549 nm and from 1538 to 1534 nm, when the oxygen concentration increases from 0 to 30 at. %. No further changes are noticeable for [O]>30 at. %. This leads to the conclusion that the bonding environment of the Er ions in annealed *a*-SiO_x:H changes for oxygen contents 0<[O]<30 at. %. Nevertheless, the intensity of the Er^{3+} PL at 77 K does not show significant changes as a function of the oxygen content. Thus, it seems that after adequate annealing, even smaller amounts of oxygen (below 1 at. % for the shown *a*-Si:H sample) approximately satisfy the requirement of an erbium surrounding with sufficiently low symmetry for efficient luminescence. Furthermore, other studies on *a*-Si:H(Er) have suggested that the oxygen content and correspondingly the Er environment are not the most important factors for the PL enhancement in disordered Si, but that the main effect is rather a structural modification of the network that may lead to a reduction of defects and an improvement of the energy transfer.[36,42] Unfortunately, a detailed analysis of the Er environment is not possible in *a*-SiO_x:H. The intrinsic disorder in the layers leads to random variations of the local bonding structure and stoichiometry (e.g., network position of oxygen atoms and local hydrogen content). This gives rise to a statistical broadening of the Er transition (full width at half maximum $\approx$10–15 meV), which is larger than that in crystalline hosts.[43,44] As a consequence, similar studies as for *c*-Si(Er) are difficult in our case. Restrictions also exist for a structural investigation by extended x-ray absorption fine structure since this technique does not allow us to clarify the influence of hydrogen atoms.

The right half of Fig. 9 shows the intrinsic SiO_x PL of the Er-implanted, annealed samples (solid curves), and additionally of an unimplanted, as-deposited set of samples (dashed curves) with the same oxygen contents. The peak energy of the as-deposited SiO_x PL (dashed curves) is shifted from roughly 1.3 to 1.75 eV when [O] is increased, corresponding to an increase of the optical gap E_{04} from 1.9 to 2.7 eV. The increasing energy difference between E_{04} and the PL maximum represents the energetic distribution of the band-tail states involved in the intrinsic PL. Photoexcited charge carriers first thermalize into the band tails before they recombine radiatively.[11] In addition, a broadening of the intrinsic PL can be seen for higher [O], again due to the broader tails.

The main difference between the SiO_x PL spectra of implanted compared to unimplanted samples is a decrease of the PL peak energy by roughly 0.2–0.3 eV. In comparison to the unimplanted state, strong implantation leads to additional disorder in the samples that cannot be annealed out completely. Thus, photogenerated charge carriers can thermalize into deeper band-tail states and the PL peak energy is accordingly smaller. This tail broadening can already be identified

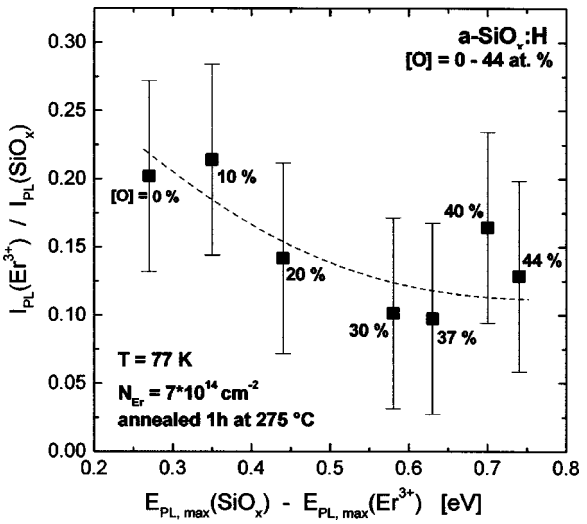

FIG. 10. Ratio of the Er^{3+} and the SiO_x PL intensities $I_{PL}(Er^{3+})/I_{PL}(SiO_x)$ at 77 K as a function of the energy difference between the two PL maxima $E_{PL,max}(SiO_x)-E_{PL,max}(Er^{3+})$. The samples have oxygen concentrations between 0 and 44 at. %, were multi-implanted with an Er dose of $N_{Er}=7\times10^{14}$ cm^{-2} and annealed afterwards at 275 °C for 1 h. The line is a guide to the eye.

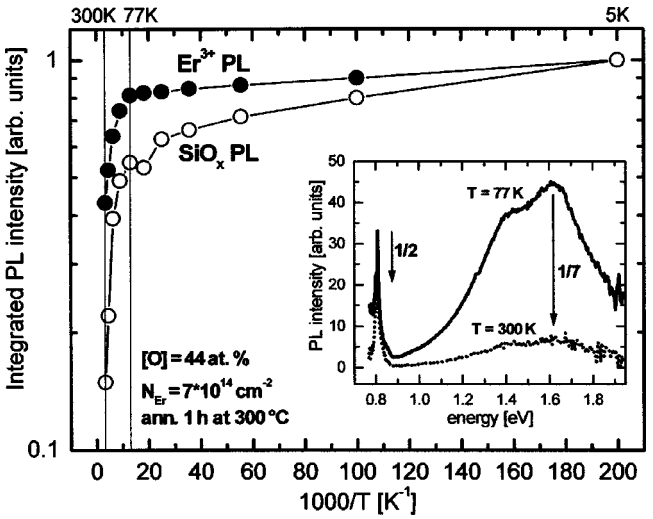

FIG. 11. Normalized SiO_x and Er PL intensities of an a-SiO_x:H sample with 44 at. % oxygen and a band gap of 2.7 eV as a function of the inverse temperature. The sample was multi-implanted with an Er dose of $N_{Er}=7\times10^{14}$ cm^{-2} and annealed afterwards at 300 °C for 1 h. The lines are guides to the eye. The inset shows intrinsic and Er PL spectra of the same sample at 77 and 300 K. The quenching factors for both PL are indicated next to the arrows.

in Fig. 2(d) as a shift of the band-tail absorption of the annealed implanted samples to lower photon energies by approximately 0.2 eV. Note that the shoulders at roughly 1.4 eV, which can be seen in some of the PL curves in Fig. 9, arise from a distinct spectral feature in the response of the detection system, which could not be removed completely and has no special significance. Also, no intrinsic defect luminescence was observed in any of the PL spectra at 77 K.

The fact that the Er^{3+} PL intensity is rather insensitive to the increase of the optical gap with increasing [O], whereas tail-to-tail transitions of course change their average energy depending on the band gap (as seen in Fig. 9), leads to the question, which transitions are responsible for the excitation of the first excited Er state? In particular, the energy separation of the Er^{3+} and the SiO_x PL peaks becomes larger with increasing oxygen content, without causing a decrease of the Er^{3+} PL intensity. This qualitatively contradicts a direct resonant excitation of the erbium $^4I_{15/2}\rightarrow{}^4I_{13/2}$ transition via SiO_x tail-to-tail recombination. In Fig. 10, the ratio of the Er^{3+} and the SiO_x PL intensities $I_{PL}(Er^{3+})/I_{PL}(SiO_x)$ is plotted as a function of the difference between the two PL maxima $E_{PL,max}(SiO_x)-E_{PL,max}(Er^{3+})$. By using this ratio, the dependence of the luminescence intensity on the different defect densities for the different oxygen contents is eliminated to first order and a direct comparison is possible. There is a small decrease of $I_{PL}(Er^{3+})/I_{PL}(SiO_x)$ with increasing [O], but it only comprises a factor of about 2 for [O] $=0-44$ at. %. If resonance or only approximate resonance between intrinsic and erbium PL at 0.8 eV were required for the energy transfer, this weak dependence would not seem consistent with the large energy separation of $E_{PL,max}(SiO_x)$ $-E_{PL,max}(Er^{3+})=0.75$ eV at the highest oxygen content. This suggests that other mechanisms, such as the energy transfer to higher excited Er levels such as $^4I_{11/2}$, may significantly contribute to the excitation of the rare-earth-ion PL at 0.8 eV. As a matter of fact, there is a considerable spectral overlap of the intrinsic SiO_x PL with the transition energy from the Er^{3+} ground state to the second excited state ($^4I_{15/2}\rightarrow{}^4I_{11/2}$) at 1.265 eV (980 nm), as indicated by a dashed line in Fig. 9. Further details will be discussed below.

Figure 11 displays the Er and SiO_x PL intensities as a function of the inverse temperature. The sample contains 44 at. % oxygen, is highly implanted, and was annealed at 300 °C for 1 h. There is a clear difference between the temperature dependencies of the two luminescence intensities. The thermal quenching of the intrinsic PL starts at lower temperatures and is more pronounced than that of the Er PL. For example, the inset of Fig. 11 shows that for increasing temperature from 77 to 300 K the intrinsic PL is quenched by a factor of 7, whereas the Er PL is only reduced by a factor of 2. Similar differences between host and rare-earth-ion PL have been observed also by others for Er-doped amorphous host materials such as a-Si:H, a-SiO_x:H, and a-$Si_{1-x}C_x$:H.[10,28,32,40,45] In general, the extent of the thermal quenching depends on the material properties and is smaller for larger band gaps (higher [O]) and correspondingly broader band tails (see Fig. 12). Kühne *et al.*[28] for their a-Si:H(Er) samples detected not only the intrinsic and the Er PL but also the deep-defect-related PL at about 0.9 eV. It displayed a temperature quenching similar to the Er PL, which lead to the conclusion that the Er excitation mechanism is defect-related. However, for none of the silicon suboxides studied here is a defect-related PL close to the Er peak detected (see Fig. 9). Thus, the results of Ref. 28 cannot be generalized to a-SiO_x, where the luminescence intensity of Er is even higher. In fact, the Er PL is still quite strong at 300 K, when most of the SiO_x luminescence has vanished. This demonstrates that the excitation of Er ions has only a minor influence on the SiO_x PL, which is determined by other pro-

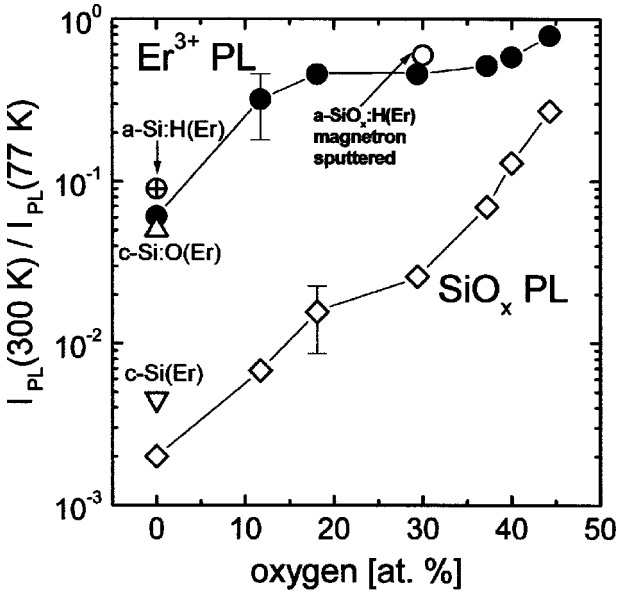

FIG. 12. Temperature quenching of SiO_x and Er^{3+} PL from 77 to 300 K for oxygen contents from 0 to 44 at. %. The erbium implantation dose was 7×10^{14} cm^{-2} ($\approx10^{20}$ cm^{-3}). The samples were annealed at 275 °C for 1 h. The lines are guides to the eye. Also shown for comparison is the thermal quenching of the Er^{3+} PL ($N_{Er}=10^{19}$ cm^{-3}) in crystalline silicon with and without codoping by oxygen (10^{20} cm^{-3}) (Ref. 4), in a-Si:H(Er) (Ref. 45), and for a magnetron-sputtered a-SiO_x:H(Er) sample ($N_{Er}\approx4\times10^{19}$ cm^{-3}) (78). The uncertainties of the quenching factors are shown by an error bar on one of the data points for each data set.

cesses such as nonradiative recombination.

In order to be efficient and stable at room temperature, the thermal quenching of the Er luminescence in the respective host has to be minimized. This can be achieved by a favorable Er^{3+} environment that reduces the radiative lifetime, or by an increase of the host band gap that prevents the deexcitation of Er ions via backtransfer of the excitation energy to the host matrix. The thermal quenching of the SiO_x and Er PL from 77 to 300 K [$I_{PL}(300\ K)/I_{PL}(77\ K)$] as a function of oxygen content is displayed in Fig. 12. The quenching of the SiO_x PL for [O] ranging from 0 to 44 at. % is considerably reduced as the oxygen content increases. For [O] $=0$ at. %, the quenching is about three orders of magnitude and decreases to a factor of 3 at [O]$\approx$44 at. %. This can be understood from the widening of the optical gap and the increased density of deep localized band-tail states, already known for unimplanted a-SiO_x:H.[11,46]

In crystalline Si,[4] the Er^{3+} PL is quenched between 77 and 300 K by $2\frac{1}{2}$ orders of magnitude (Fig. 12). Co-doping with oxygen,[4] however, results in a quenching by only $1\frac{1}{2}$ orders of magnitude, a value comparable to a-Si:H(Er),[28,45] which always contains residual small amounts of oxygen ($<$1 at. %). In comparison to these host materials, the erbium luminescence in a-SiO_x:H is quenched much less. Starting from a quenching of $1\frac{1}{2}$ orders magnitude for [O] <1 at. %, the reduction factor $I_{PL}(300\ K)/I_{PL}(77\ K)$ is only 0.8 at the highest oxygen content studied here (44 at. %). This is in good agreement with values obtained in Er-doped

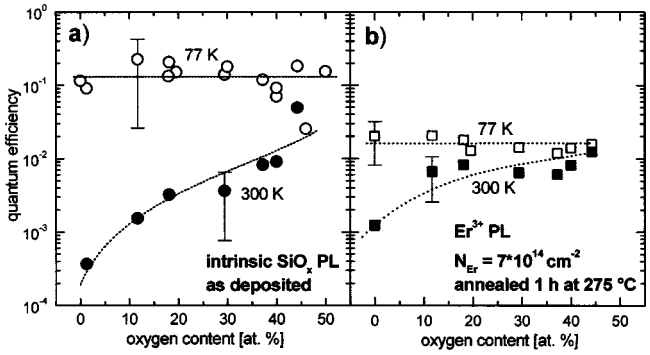

FIG. 13. Quantum efficiencies at 77 and 300 K as a function of [O], for (a) the intrinsic PL of unimplanted, as-deposited SiO_x samples and (b) for the Er^{3+} PL of samples, which were multiimplanted with an Er dose of $N_{Er}=7\times10^{14}$ cm^{-2} and annealed afterwards at 275 °C for 1 h. The lines are guides to the eye.

semi-insulating polycrystalline silicon[12] (SIPOS) and magnetron-sputtered a-SiO_x:H(Er), which also contain large oxygen concentrations.

Qualitatively, the Er^{3+} PL thermal quenching shows the same tendency as that of the intrinsic PL, but it is significantly smaller for all oxygen concentrations and also has a smaller variation with oxygen content. Thus, a major benefit of increasing oxygen alloying is the significant reduction of the thermal quenching of the Er^{3+} PL (and of the SiO_x PL, as well). With the knowledge of the relative PL intensities (Fig. 9) and using a suitable calibration procedure, the quantum efficiencies η of the SiO_x and Er^{3+} PL at an excitation wavelength of 458 nm can be estimated. Starting from known values of η for a-Si:H and taking into account the different defect densities and the observed quenching at the respective temperatures,[35,46,47] the quantum efficiencies for both PL at 77 and 300 K were estimated and are shown in Fig. 13. The SiO_x quantum efficiency [Fig. 13(a)] was determined for the as-deposited unimplanted set of samples (dashed curves in Fig. 9). At 77 K, $\eta(SiO_x)$ is roughly 0.1 for all oxygen contents, whereas at room temperature, the oxygen dependence of the PL quenching results in an increase of $\eta(SiO_x)$ over two orders of magnitude from below 10^{-3} for [O]$<$1 at. % to above 10^{-2} for [O]$=$44 at. %. The PL quantum efficiency of Er^{3+} [Fig. 13(b)] in the highly implanted annealed SiO_x samples (solid curves in Fig. 9) is in the range of 0.01–0.02 at 77 K and shows no significant variation with oxygen content. At 300 K, $\eta(Er^{3+})$ is reduced to values around 10^{-3} for [O]$<$10 at. %, but reaches a value of approximately 0.01 for [O]$>$15 at. %.

3. Influence of higher-level Er^{3+} transitions and excitation efficiency

Although the most desirable transition for applications of Er ions in Si is the one from the first excited state $^4I_{13/2}$ to the ground state $^4I_{15/2}$ ($\lambda=1.54\ \mu$m), also transitions from or to the higher levels $^4I_{11/2}$ and $^4I_{9/2}$ can be observed under appropriate conditions. Transitions from the second and third excited state to the ground state ($^4I_{11/2}\rightarrow{}^4I_{15/2}$ and $^4I_{9/2}\rightarrow{}^4I_{15/2}$) result in luminescence lines at about 1.265 eV

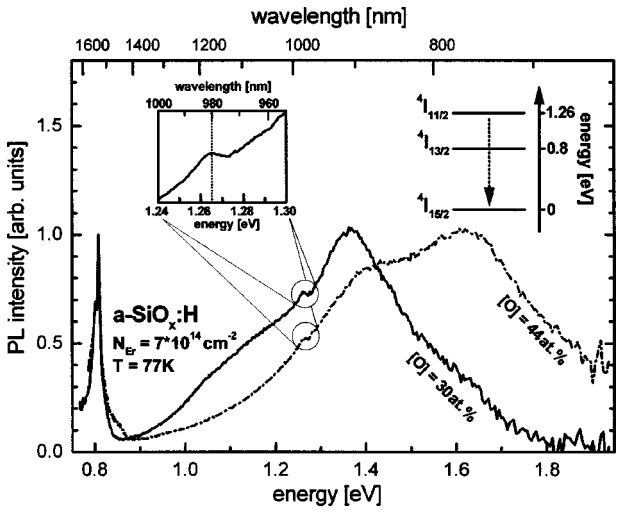

FIG. 14. Er and SiO_x PL spectra of samples containing 30 and 44 at. % oxygen ($N_{Er}=7\times10^{14}$ cm^{-2}, annealed 1 h at 300 °C) at 77 K. The inset shows the spectral feature at 1.265 eV (980 nm), which is situated on top of the intrinsic luminescence and originates from the transition of the second excited to the Er^{3+} ground state $^4I_{11/2}\rightarrow{}^4I_{15/2}$.

(=980 nm) and 1.55 eV (=800 nm). As a matter of fact, in erbium-doped optical fiber amplifiers a population inversion of the first excited state $^4I_{13/2}$ is generated by pumping the Er ions embedded in the fibers either directly at 1.5 μm or via the second excited state $^4I_{11/2}$.[48–50] So far, evidence for higher-level Er transitions has been reported only in a few previous publications, where Si (Er) nanocrystals were embedded in *a*-Si:H (Ref. 32) or SiO_2 films (Refs. 51–53).

For the erbium-implanted *a*-SiO_x:H samples studied here, Fig. 14 shows a spectral feature at 1.265 eV (980 nm) superimposed on the intrinsic PL, which can be seen on all PL curves of highly-Er-implanted and annealed samples, irrespective of the oxygen content. At closer inspection, it actually can be identified in all PL spectra of Fig. 9 (solid curves), as well. Its origin is the transition from the second excited state to the ground state of the Er 4*f* shell $^4I_{11/2}\rightarrow{}^4I_{15/2}$, schematically depicted in Fig. 14. There are two possible explanations for the excitation of this transition. One possibility is that the energy of a tail-to-tail transition in the SiO_x matrix is transferred more or less effectively to the Er ion and excites the $^4I_{11/2}$ state. This would imply that the intrinsic luminescence is quenched to a certain extent at energies slightly higher than 1.265 eV, which should lead to a Fano-type spectrum.[54] On the other hand, also an upconversion process involving two Er ions is possible. Such an Er-Er interaction is known from Er-doped Y_2O_3, Al_2O_3, yttrium aluminum garnet YAG and glasses such as soda-lime silicate and phosphosilicate glass.[55] Here, the energy of the 0.8-eV Er transition ($^4I_{13/2}\rightarrow{}^4I_{15/2}$) is transferred nonradiatively to another Er atom (already in the $^4I_{13/2}$ state), which is thereby excited into the third excited $^4I_{9/2}$ state. From there, thermalization occurs to the $^4I_{11/2}$ level and radiative recombination with $\lambda=980$ nm takes place. Unfortunately, the small signal intensity of this transition on the background of the large intrinsic SiO_x PL does not allow a definitive identification of the relevant excitation process. No such resonant feature is observed for the $^4I_{9/2}\rightarrow{}^4I_{15/2}$ transition at 800 nm (1.55 eV).

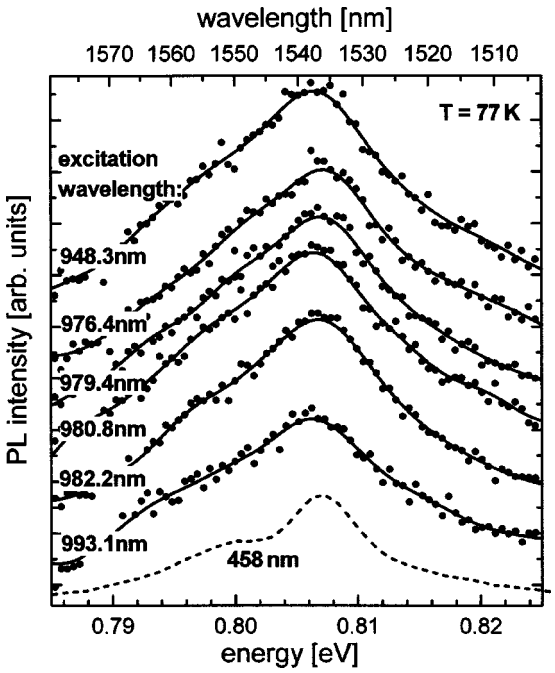

FIG. 15. Spectra of the 1.54-μm Er PL for different excitation wavelengths between 948 and 993 nm ($T=77$ K). The data are corrected for the pump intensity at the respective λ_{exc}. The solid lines result from a smoothing of the spectra. For comparison the Er luminescence at $\lambda_{exc}=458$ nm is shown as well (not corrected for λ_{exc}). The SiO_x sample contains 20 at. % oxygen, was highly Er implanted ($N_{Er}=7\times10^{14}$ cm^{-2}), and was annealed for 1 h at 275 °C.

Although higher-level Er transitions have so far mainly been seen in host materials containing Si nanocrystals,[32,51–53] there are no indications for nanocrystals in our *a*-SiO_x:H samples, which are deposited at conditions where the material growth is amorphous. Subsequent to deposition, the material was only subjected to annealing temperatures below 300 °C, where hydrogen is the only mobile component. No evidence of nanocrystalline Si (nc-Si) PL can be seen in any of the *a*-SiO_x:H spectra. Also, the Er and *a*-SiO_x PL have qualitatively similar temperature dependences, which correlate well with the oxygen content of the *a*-SiO_x host (see Fig. 12). Thus, we conclude that the observation of higher excited Er^{3+} states in *a*-SiO_x:H(Er) is independent of the formation of Si nanocrystals.

In order to find out whether the second excited erbium state $^4I_{11/2}$ acts as an intermediate state for the population of the $^4I_{13/2}$ level, a SiO_x sample with 20 at. % oxygen was excited with resonant sub-band-gap light from a Ti-sapphire laser ($\lambda_{exc}=920-995$ nm). Despite the weak absorption of the sample in this energy range, the main Er PL (at 1.54 μm) could still be detected. In the spectra of Fig. 15, there is no abrupt change of the Er PL intensity when the excitation wavelength was tuned from values lower to values higher than 980 nm (=1.265 eV, $^4I_{15/2}\rightarrow{}^4I_{11/2}$). Previous results[10,28,45] also reported no enhancement of the 1.54-μm

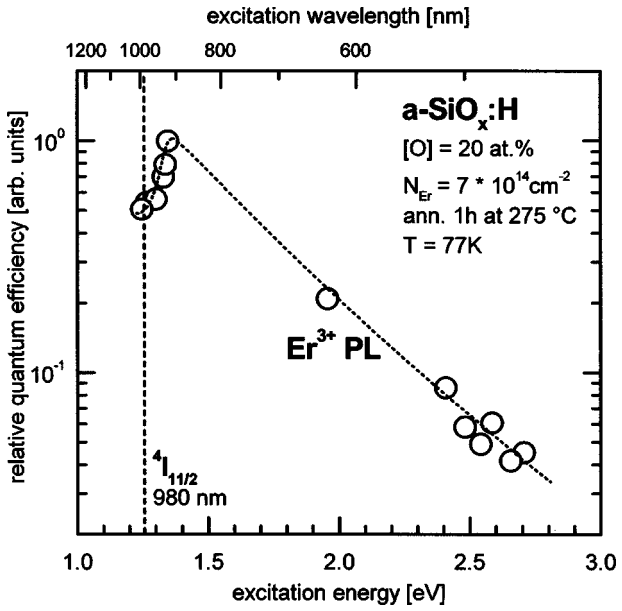

FIG. 16. Relative quantum efficiency (Er^{3+} PL intensity at 77 K normalized to the amount of absorbed photons) as a function of excitation energy. The SiO_x:H sample contains 20 at. % oxygen, was implanted with an Er fluence of 7×10^{14} cm^{-2}, and was annealed for 1 h at 275 °C. The Er PL at 1.54 μm was excited with an Ar-ion laser (458–514 nm), a He-Ne laser at 632 nm and a Ti-sapphire laser (920–995 nm). The dashed vertical line indicates the position of the second excited Er^{3+} level $^4I_{11/2}$. The dotted line is a guide to the eye.

Er PL around $\lambda_{exc}=980$ nm, which agrees well with the lack of direct light absorption by erbium ions in the absorption spectra. However, for a population of the erbium $^4I_{11/2}$ level via the SiO_x matrix, a Stokes shift is very likely to exist between the absorption of the SiO_x matrix and the energy, at which excitation to the $^4I_{11/2}$ level occurs.

At 1.265 eV (980 nm), there is a strong spectral overlap of the second excited Er level with the SiO_x PL for all [O] (indicated by a dotted line at 980 nm in Fig. 9). Therefore, a population of the first excited Er level $^4I_{13/2}$ via the second excited level $^4I_{11/2}$ is a possible contribution to the 0.8-eV Er^{3+} PL. For [O]$<$20 at. %, there also exists a resonant overlap of the broad intrinsic SiO_x PL with the first excited $^4I_{13/2}$ Er level (0.8 eV; see Fig. 9), which has been discussed as an important mechanism for resonant Er excitation in the case of *a*-Si:H. This partial overlap, however, is reduced and finally is negligible for larger oxygen contents, which should result in a strong decrease of the Er PL with rising [O] (cf. discussion of Fig. 10). However, the ratio $I_{PL}(Er^{3+})/I_{PL}(SiO_x)$ decreases only by a factor of 2 in Fig. 10. Thus, other pathways for the excitation of the first excited Er $^4I_{13/2}$ level, presumably via the second excited $^4I_{11/2}$ state, are likely to contribute at higher [O].

Evidence for a direct excitation of the $^4I_{15/2}\rightarrow{}^4I_{11/2}$ transition via the SiO_x matrix can be found in Fig. 16, which shows the excitation efficiency of the erbium luminescence for an annealed highly implanted SiO_x with 20 at. % oxygen at 77 K. The data were obtained by normalizing the intensity of the Er^{3+} PL to the flux of absorbed photons at the respective excitation wavelengths. The relative Er^{3+} PL quantum efficiency is more than one order of magnitude larger for sub-band-gap excitation between 1.2 and 1.3 eV than for band-to-band absorption around 2.5 eV. There is an increase by a factor of 2 for excitation energies slightly above 1.265 eV (980 nm), which allows us to quantify the contribution of the second excited Er level to the 0.8-eV Er PL in these samples. As conjectured above, a Stokes shift of at least 0.1 eV exists between the most favorable excitation energy and the erbium $^4I_{15/2}\rightarrow{}^4I_{11/2}$ transition at 1.265 eV. This additional excitation path, contributing at all [O], can also explain the weak decrease of the Er PL intensity with increasing oxygen content (cf. Figs. 9 and 10). A similar enhancement of the Er PL for sub-band-gap excitation has also been reported by Fuhs *et al.* for *a*-Si:H(Er).[45] Based on the estimated absolute quantum efficiencies for excitation of the Er^{3+} PL with 458-nm laser light (roughly 1% at 77 K, cf. Fig. 13) and the relative spectral dependence of η in Fig. 16, we obtain a total quantum efficiency for Er^{3+} in *a*-SiO_x:H at 77 K close to 10% for excitation at 970 nm.

Owing to the already large parameter space we have not performed detailed excitation spectroscopy measurements for all [O], which nevertheless is an interesting topic for future studies. This would allow us to quantify the contribution of the different Er^{3+} levels as a function of their resonance with the intrinsic SiO_x PL (as adjusted by the optical gap E_{04} and [O], respectively). However, as seen in Figs. 9 and 10, the Er PL intensity decreases weakly as a function of [O], which suggests that such an optimized overlap between the Er levels and the broad SiO_x PL band only would have a minor influence.

IV. DISCUSSION

Due to the fact that its 1.54-μm luminescence is rather independent of the host matrix, Er^{3+} has been incorporated into a large number of host systems. The respective excitation mechanisms for the desired Er^{3+} PL turn out to differ considerably depending on the host properties. Erbium embedded in SiO_2 fibers can be directly excited by means of resonant pumping,[27,48–50] whereas in crystalline and amorphous semiconductors the excitation prevalently occurs via absorption by the host and subsequent energy transfer to the rare-earth ions. In the case of *c*-Si, erbium is believed to be excited by an Auger process. An electron from the conduction band is trapped at an Er-related level (0.15 eV below the conduction-band edge). After recombination with a hole the energy is transferred to the Er ion by means of an Auger effect.[56–60] Auger recombination has also been reported as an excitation mechanism for Er in III-V semiconductors such as In-Ga-P (Ref. 61) or Al-Ga-As (Ref. 62). Interactions of excitons and rare-earth-metal ions have been observed in $CsCdBr_3$, as well.[63] In amorphous materials, the determination of the Er^{3+} excitation mechanism is more complicated due to the larger density and variety of tail and defect states that are located in the band gap. Luminescence from erbium ions has so far been detected in hydrogenated *a*-Si and its alloys *a*-SiO_x and *a*-SiC_x,[28] but also in chalcogenide glasses[64] or sputtered *a*-GaN.[65] The energy-transfer mecha-

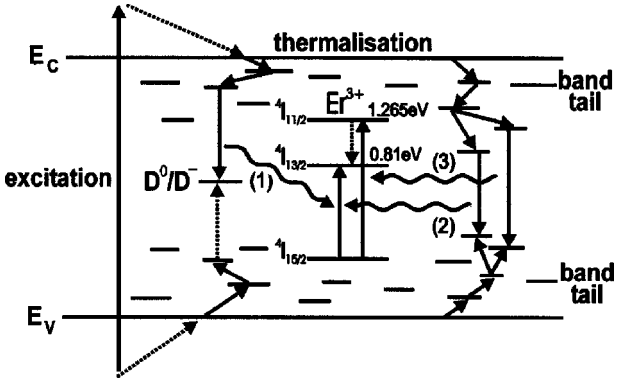

FIG. 17. Schematic diagram of possible transitions leading to the excitation of the $^4I_{13/2}$ Er^{3+} level via the amorphous a-SiO_x host matrix. Process (1) shows a defect-related excitation of the erbium $^4I_{13/2}$ level caused by a transition of a conduction-band tail electron to a dangling-bond defect (D^0/D^-). Process (2) represents an excitation of the $^4I_{13/2}$ state via tail-to-tail recombination from deep localized band-tail states and in process (3) the first excited Er state $^4I_{13/2}$ is populated via an excitation of the second excited erbium state $^4I_{11/2}$.

nisms, however, are still under discussion. For the case of amorphous silicon, two different excitation models have been suggested:

(i) Fuhs *et al.*[45] and Yassievich, Bresler, and Gusev[66] proposed a defect-related Auger effect (DRAE) as the main excitation path of Er^{3+} in a-Si:H. An electron from the conduction-band tail is captured by a neutral dangling-bond defect state and excites an Er^{3+} ion ($^4I_{15/2}\rightarrow{}^4I_{13/2}$) by a nearly resonant Auger process (process 1 in Fig. 17). This occurs in competition with radiative recombination [leading to a defect PL band around 0.9 eV (Ref. 28)] and a nonradiative multiphonon process. This model is based on the close vicinity of Er ions and dangling-bond defects that are supposed to be introduced in large numbers as a result of erbium incorporation in the amorphous matrix. The model is supported by the similar temperature quenching of the defect and Er luminescence and by the fact that the temperature quenching of the rare-earth-ion PL can be simulated quite well based on the competition between the DRAE excitation process and nonradiative multiphonon recombination at defects. A band-tail–to–band-tail Auger recombination, exciting the Er $^4I_{13/2}$ via the $^4I_{11/2}$ state is unlikely because of the different temperature dependence of the intrinsic a-Si PL at 1.3 eV and the Er luminescence.

(ii) The second model for Er excitation is a dipole-mediated resonant energy transfer originally proposed by Förster[67,68] for the interaction of molecules in gases and liquids. This mechanism is also evoked for the energy transfer in photosynthesis[69] and between semiconductor quantum structures and organic matrices.[70,71] In rare-earth doped a-Si:H, it resembles a resonant Auger transfer and is efficient for large distances up to 50 Å—as suggested by Kühne *et al.*[28] The necessary dipole moment of the Er^{3+} ion is provided by local fields in its surroundings, i.e. the oxygen atoms are situated close by. For tetrahedrally coordinated amorphous silicon, the conduction-band and band-tail states exhibit predominant s character, whereas valence-band and band-tail states as well as dangling-bond states have p character. Thus, the required dipole moment in the a-Si host is provided by electron-hole pairs. In contrast to the DRAE, where excess recombination energy can be taken up by phonons, resonance is necessary for a Förster transfer, which of course narrows the energetic window for efficient excitation. On the other hand, this mechanism does not require a close proximity of Er and dangling bonds. Since the Er concentration in amorphous hosts is generally one to two orders of magnitude higher than the defect concentration, an overall close neighborhood of Er and defects is unlikely. Thus, a transfer over larger distances is more favorable and explains the observed threshold for the detection of Er PL, namely, when the transfer distance exceeds 50 Å at low Er concentrations ($\approx 10^{18}$ cm^{-3}). These considerations imply that not only transitions involving defects (process 1 in Fig. 17) but also transitions between deep localized tail states (processes 2 and 3 in Fig. 17) can play a role for the Er excitation.

A third possible excitation path is the existence of charge-transfer levels of Er^{3+} in the bands or the band gap of the amorphous host material. Little insight exists so far in the electronic structure of Er in Si hosts and most theoretical work has concentrated on Er in c-Si. Depending on how strong the bonding and interaction of Er^{3+} with its surroundings is, the resulting energy of the Er $4f$ levels ranges from far below the band gap ($\sim$20 eV) to a position directly in the band gap of c-Si.[58,72–75] As far as amorphous silicon is concerned, recent experimental results by Tessler *et al.*,[76] using ultraviolet photoemission spectroscopy (UPS) on a-Si:H(Er) samples, found a binding energy E_B, attributed to the Er^{3+} $4f$ levels, which is roughly 10 eV below the Si valence-band maximum. This feature in the UPS spectra, however, could only be seen as a rather weak peak at high excitation photon energy (140 eV). It cannot be excluded that other Er $4f$–related peaks with smaller binding energies exist in the UPS spectra, which are too weak to be resolved. Such levels might be energetically closer to the band maxima or the gap and could therefore allow for a direct excitation of the rare-earth ions by charge transfer from the amorphous host material.

For the evaluation of the relevant excitation mechanism of Er^{3+} in a-SiO_x:H, the following experimental observations have to be taken into account:

(i) No direct absorption of the erbium ions at resonant transitions between Er^{3+} levels ($^4I_{15/2}\rightarrow{}^4I_{13/2}$ at 0.8 eV and $^4I_{15/2}\rightarrow{}^4I_{11/2}$ at 1.265 eV) could be observed in absorption spectra. Thus, Er ions are excited mainly by an energy transfer from the SiO_x matrix.

(ii) The thermal quenching is roughly one order of magnitude smaller for the Er^{3+} PL than for the intrinsic SiO_x PL. There is a comparable reduction of the quenching for both PL with increasing [O] since the reexcitation of charge carriers into the bands is more unlikely for samples with higher [O], which possess deeper tail states (Fig. 12). But, generally, there is a large quantitative difference in the temperature quenching of Er and SiO_x PL. In particular, for low oxygen contents ($[O]\leqslant 10$ at. %), Er PL can still be observed at 300

K, when the intrinsic recombination is almost completely quenched.

(iii) Upon sub-band-gap excitation, i.e., in the absence of band-to-band absorption as well as intrinsic tail-to-tail recombination, the 1.54-μm Er luminescence is still detectable, with a quantum efficiency approximately one order of magnitude higher than that for band-to-band pumping (see Figs. 15 and 16). An additional resonant increase of the Er^{3+} PL by approximately a factor of 2 was observed for pumping slightly above 1.265 eV (980 nm), the transition energy from the erbium ground state to the second excited state ($^4I_{15/2} \rightarrow {}^4I_{11/2}$).

(iv) There is an inverse correlation between the density of defects in the host and the intensity of the Er^{3+} PL, i.e., the PL is significantly increased when defects are reduced by appropriate annealing (Fig. 6). Also, an incorporation into more favorable Er-O environments seems to occur upon annealing (Fig. 8). Furthermore, the erbium peak concentration is around 10^{20} cm^{-3}, whereas the defect density is 1–2 orders of magnitude lower (10^{18}–10^{19} cm^{-3}) in annealed samples.

Among these results, points (i) and (ii) agree very well with DRAE. In *a*-Si:H(Er), Fuhs *et al.*[45] found an intrinsic defect PL at roughly 0.9 eV with a thermal quenching similar to the Er^{3+} PL. These authors suggested that defect-related transitions in *a*-Si:H were the dominant process in the excitation of erbium ions (DRAE, process 1 in Fig. 17). However, no such defect PL is detectable in amorphous suboxides. Even in our *a*-Si:H(Er) samples, it cannot be resolved due to the large intensity of the erbium luminescence at 0.8 eV.

As for point (iii), a higher Er^{3+} PL excitation efficiency for sub-band-gap-pumping has also been found by Fuhs *et al.*[45] and does not contradict the DRAE model. However, unlike in *a*-SiO_x, no contribution of the $^4I_{11/2}$ Er level to the population of the $^4I_{13/2}$ level has been observed in *a*-Si:H. Thus, the conclusions of the DRAE model cannot be readily transferred to the case of *a*-SiO_x:H(Er). Other possible excitation pathways of Er^{3+} in silicon suboxides have to be taken into account.

An important argument against the DRAE applies also in the case of Er^{3+}-implanted SiO_x:H [item (iv)]. The Er ions outnumber the defect states by 1–2 orders of magnitude and the Er PL intensity increases almost linearly with the total Er concentration (Fig. 8). This is incompatible with a one-to-one correlation of active erbium atoms and dangling bonds throughout the sample. Similarly, it is difficult to explain by DRAE that annealing reduces the number of defects by almost one order of magnitude and at the same time the Er^{3+} PL is strongly enhanced—as shown in Fig. 6. Last but not least, the DRAE model does not consider the role of Er-O complexes, which exist in *a*-SiO_x and to a smaller extent in *a*-Si, as well. Tessler *et al.*[40] suggested that these complexes might help to increase the number of defect states around the erbium ions. This, however, would require the existence of two types of defects, one that is associated with Er-O complexes and another that represents the ordinary *a*-Si:H dangling bond. So far, there is no spectroscopic evidence for such a second type of defect.

In contrast to the DRAE model, most of the experimental findings for erbium in amorphous silicon suboxides can be reasonably explained in the framework of a Förster transfer. Such a dipole-mediated process can occur over larger distances (up to 50 Å). Thus, the existence of an Er threshold concentration can be explained. The Er density in the host should be large so that the distance between an Er atom and the electron-hole dipoles (which transfer the excitation energy) is smaller than 50 Å. For defect-related transitions (process 1 in Fig. 17)—if contributing to the energy transfer to Er^{3+}—neither a close vicinity nor equal numbers of Er^{3+} ions and defects are required. Moreover, the Förster mechanism opens the possibility of alternative excitation pathways, which—unlike defect-related transitions—do not contradict the observation that annealing enhances the erbium PL while simultaneously reducing the defect density. Transitions between deep localized conduction- and valence-band tail states are likely to excite the Er $^4I_{13/2}$ (0.8 eV) and $^4I_{11/2}$ (1.265 eV) states (processes 2 and 3 in Fig. 17). In this case, annealing helps to reduce nonradiative recombination paths via defects and makes process 2 and 3 more likely. This assumption is corroborated by the finding of a resonant enhancement of the 0.8-eV Er PL (according to process 3 in Fig. 17) when the pump wavelength approaches resonance with the second excited erbium level (Fig. 16).

One condition required by a Förster process is resonance between the exciting electron-hole dipole and the excited rare-earth ion. It was shown in Fig. 9 that for oxygen contents below 15 at. %, the SiO_x PL overlaps partly with the first excited state of erbium $^4I_{13/2}$ at 0.8 eV. In addition, there is always a sufficient overlap of the intrinsic PL with the second excited erbium state $^4I_{11/2}$ at 1.265 eV, which prevents a strong decrease of the Er^{3+} PL at larger [O], when resonance at 0.8 eV is unlikely (see Fig. 10). Note, however, that the temperature quenching is one order of magnitude weaker for the rare-earth-ion PL than for the intrinsic PL in both host materials, *a*-Si:H and *a*-SiO_x:H. On the other hand, the Er^{3+} excitation process at the resonance energies is not necessarily expected to correlate strongly with the SiO_x PL or its quenching. Even at temperatures where the intrinsic PL is almost completely quenched due to reexcitation of trapped charge carriers into the bands, the energy transfer from deep band-tail states to Er^{3+} can still be faster and more effective, which should lead to a weaker thermal quenching by nonradiative recombination processes. The small size of the spectral feature at 1.265 eV, superimposed on the SiO_x PL spectra (see Fig. 14), could indeed be an indication for the minor influence of the Er excitation processes on the SiO_x PL.

We conclude that the interpretation of the experimental results in the framework of a defect-related model (DRAE) leads to several inconsistencies concerning the energy-transfer process from the *a*-SiO_x:H host to the Er^{3+} ions. On the other hand, most of these contradictions can be reasonably resolved by a dipole-mediated Förster mechanism. A certain contribution from defect states or from Er^{3+} charge-transfer levels in vicinity of the band gap, however, cannot be entirely excluded.

The presented results also have some relevance for other

Er-doped Si-O systems, e.g., those that are partially crystallized[12] (SIPOS) or contain Si-nanocrystals (nc-Si) embedded in a (sub)oxide matrix.[14–17,32,51–53] In these materials, Er^{3+} is likely to be located in the vicinity of the disordered Si-O phase, which is believed to surround the Si crystallites.[16] Correspondingly, one common feature of the Er PL in all these hosts (a-SiO_x:H, SIPOS, nc-Si) is the similar broad luminescence that only allows one to distinguish two main transitions ($\approx$1538 and 1550 nm) and thus differs significantly from the well-resolved spectra obtained for c-Si(Er). But also the Er^{3+} PL temperature quenching (from 77 to 300 K) of SIPOS (Ref. 12) and nc-Si (Ref. 17) is less than a factor of 10, which agrees quite well with the findings presented in this article (cf. Fig. 12) and points towards a reduced backtransfer due to larger optical band gaps. Furthermore, SIPOS samples containing comparable amounts of erbium as SiO_x show a similar activation of their luminescence upon annealing at moderate temperatures (300–400 °C). Presumably, this is due to an incorporation of Er^{3+} into a favorable oxygen environment and defect passivation. The Er PL quantum efficiency of annealed SIPOS (Er) is roughly 10^{-3}, which also compares well to the case of a-SiO_x:H(Er) (cf. Fig. 13). Unfortunately, no PL lifetime data have been recorded for our a-SiO_x:H samples so that a comparison to the respective findings for SIPOS is not possible.

On the other hand, amorphous SiO_x and partially crystallized Si-O systems are only comparable to a certain extent: First, the various deposition methods are known to produce materials with different structural properties. Second, the hydrogen content initially present in some samples effuses during the annealing procedures used for crystallization ($T > 300$ °C). Thus, the structure of the samples becomes somewhat different upon crystal formation, which complicates a direct comparison. In order to investigate the influence of Si crystallites on the rare-earth-ion luminescence, some of our a-SiO_x(Er) samples were subjected to intense Nd:YAG laser pulses ($\lambda = 355$ nm, $t_{pulse} = 8$ ns, $I_L \approx 300$ mJ/cm^2). Applying this procedure lead to the formation of Si crystallites embedded in a suboxide matrix.[77] However, no further improvement of the Er PL compared to that of amorphous samples (annealed at optimized conditions) has been observed. Nevertheless, disordered Er-doped silicon-oxygen alloys can be regarded as a model system that also provides a better understanding of the processes occurring at c-Si/a-SiO_x interfaces.

V. CONCLUSIONS

Effective erbium PL in a-SiO_x:H was detected at room temperature for varying oxygen contents and Er^{3+} peak concentrations up to 10^{20} cm^{-3}. The intensities of SiO_x and Er^{3+} PL scale inversely with the defect density and, to a smaller extent, also with the structural disorder in the host matrix. Annealing at 300 °C for 1 h was found to be optimal for the activation of both luminescence processes. Our results suggest a reconstruction of implantation-induced dangling bonds as well as an incorporation of erbium ions into more favorable environments. As there is no strong dependence of the Er^{3+} PL intensity at low temperatures on the oxygen content, already small oxygen concentrations of the order of 1 at. % seem to provide an optimal Er environment with low local symmetry. The temperature quenching of the Er^{3+} PL is roughly one order of magnitude smaller than that of the intrinsic SiO_x PL. A major advantage of alloying with increasing oxygen content is the fact that for the highest [O] the temperature quenching from 77 to 300 K is significantly reduced for both the Er (a factor of 2) and the SiO_x PL (a factor of 10). Measurements with different excitation wavelengths showed that the main Er PL at 1.54 μm is excited roughly one order of magnitude more efficiently when pumped with sub-band-gap light compared to band-to-band excitation. The excitation of Er^{3+} via the second excited level $^4I_{11/2}$ at 1.265 eV contributes to the population of the $^4I_{13/2}$ level and enhances the Er PL by a factor of 2. Based on these results, we argue that the excitation mechanism of the Er^{3+} ions in a-SiO_x:H can be explained by a resonant dipole-mediated Förster transfer to the Er $^4I_{13/2}$ and $^4I_{11/2}$ levels. On the other hand, some of the experimental findings also agree with a DRAE, whereas others do not. This casts some doubts on the relevance of the DRAE model, at least for Si-O alloys with high oxygen contents [O] > 20 at. %.

ACKNOWLEDGMENT

This work was supported by the Deutsche Forschungsgemeinschaft (Stu. 139/6-3).

*Author to whom correspondence should be addressed. Electronic address: janotta@wsi.tum.de

[1] F. G. Anderson, Appl. Phys. Lett. **68**, 2421 (1996).
[2] J. Michel, J. L. Benton, R. F. Ferrante, D. C. Jacobson, D. J. Eaglesham, E. A. Fitzgerald, Y.-H. Xie, J. M. Poate, and L. C. Kimerling, J. Appl. Phys. **70**, 2672 (1991).
[3] M. Markmann, E. Neufeld, A. Sticht, K. Brunner, G. Abstreiter, and G. Buchal, Appl. Phys. Lett. **75**, 2584 (1999).
[4] S. Coffa, G. Franzò, F. Priolo, A. Polman, and R. Serna, Phys. Rev. B **49**, 16 313 (1994).
[5] H. Ennen, G. Pomrenke, A. Axmann, K. Eisele, W. Haydl, J. Schneider, Appl. Phys. Lett. **46**, 381 (1985).
[6] B. Zheng, J. Michel, F. Y. G. Ren, L. C. Kimerling, G. C. Jacobson, and J. M. Poate, Appl. Phys. Lett. **64**, 2842 (1994).
[7] G. Franzò, F. Priolo, S. Coffa, A. Polman, and A. Carnera, Appl. Phys. Lett. **64**, 2235 (1994).
[8] T. Oestereich, S. Swiatkowski, and I. Broser, Appl. Phys. Lett. **56**, 446 (1990).
[9] M. S. Bresler, O. B. Gusev, V. Kh. Kudoyarova, A. N. Kuznetsov, P. E. Pak, E. I. Terukov, I. N. Yassievich, B. P. Zakharchenya, W. Fuhs, and A. Sturm, Appl. Phys. Lett. **67**, 3599 (1995).
[10] J. H. Shin, R. Serna, G. N. van den Hoven, A. Polman, W. G. J. H. M. van Sark, and A. M. Vredenberg, Appl. Phys. Lett. **68**, 997 (1995).
[11] R. Janssen, in *Selected Topics of Semiconductor Physics and Technology*, edited by G. Abstreiter, M.-C. Amann, M. Stutzmann, and P. Vogl (Walter Schottky Institut, Tech. Univ. Munich, 2000), Vol. 31.

[12] G. N. van den Hoven, J. H. Shin, A. Polman, S. Lombardo, and S. U. Campisano, J. Appl. Phys. **78**, 2642 (1995).
[13] R. Janssen, A. Janotta, D. Dimova-Malinovska, and M. Stutzmann, Phys. Rev. B **60**, 13 561 (1999).
[14] X. Zhao, S. Komuro, H. Isshiki, Y. Aoyagi, and T. Sugano, Appl. Phys. Lett. **74**, 120 (1999).
[15] H.-S. Han, S.-Y. Seo, and J. H. Shin, Appl. Phys. Lett. **79**, 4568 (2001).
[16] L. R. Tessler, J. L. Coffer, J. Ji, and R. A. Senter, J. Non-Cryst. Solids **299-302**, 673 (2002).
[17] M. Schmidt, J. Heitmann, R. Scholz, and M. Zacharias, J. Non-Cryst. Solids **299-302**, 678 (2002).
[18] J. F. Ziegler, J. P. Biersack, and U. Littmark, *The Stopping and Range of Ions in Solids* (Pergamon, New York, 1985), Vol. 1.
[19] W. B. Jackson, N. M. Amer, A. C. Boccara, and D. Fournier, Appl. Opt. **20**, 1333 (1981).
[20] W. Y. Ching, Phys. Rev. B **26**, 6633 (1982).
[21] R. Carius, R. Fischer, and E. Holzenkämpfer, J. Phys. C **4**, 1025 (1981).
[22] M. S. Brandt, A. Asano, and M. Stutzmann, in *Amorphous Silicon Technology—Symposium 1993*, edited by E. A. Schiff, M. J. Thompson, A. Madam, K. Tanaka, and P. G. LeComber, MRS Symposia Proceedings No. 297 (Pittsburgh, 1993), p. 201.
[23] H. Stitzl, G. Krötz, and G. Müller, Appl. Phys. A **53**, 235 (1991).
[24] A. J. M. Berntsen, W. F. van der Weg, P. A. Stolk, and F. W. Saris, Phys. Rev. B **48**, 14 656 (1993).
[25] P. A. Stolk, F. W. Saris, A. J. M. Berntsen, W. F. van der Weg, L. T. Sealy, R. C. Barklie, G. Krötz, and G. Müller, J. Appl. Phys. **75**, 7266 (1994).
[26] R. A. C. M. M. van Swaaij, A. D. Annis, B. J. Sealy, and J. M. Shannon, J. Appl. Phys. **82**, 4800 (1997).
[27] W. J. Miniscalco, in *Rare Earth Doped Fibre Lasers and Amplifiers*, edited by M. J. F. Digonnet (Dekker, New York, 1993), p. 19.
[28] H. Kühne, G. Weiser, E. I. Terukov, A. N. Kuznetsov, and V. Kh. Kudoyarova, J. Appl. Phys. **86**, 896 (1999).
[29] T. Miya, Y. Terunuma, T. Hosaka, and T. Miyashita, Electron. Lett. **15**, 106 (1979).
[30] A. Asano and M. Stutzmann, J. Appl. Phys. **70**, 5025 (1991).
[31] E. Lotter, Ph.D. thesis, Fakultät Elektrotechnik, Universität Stuttgart (1994).
[32] S. B. Aldabergenova, H. P. Strunk, P. C. Taylor, and A. A. Andreev, J. Appl. Phys. **90**, 2773 (2001).
[33] L. R. Tessler and A. R. Zanatta, J. Non-Cryst. Solids **227-230**, 399 (1998).
[34] M. Stutzmann, W. B. Jackson, and C. C. Tsai, Phys. Rev. B **32**, 23 (1985).
[35] R. A. Street, *Hydrogenated Amorphous Silicon* (Cambridge University Press, Cambridge, 1991).
[36] L. R. Tessler, C. Piamonteze, M. C. Martins Alves, and H. Tolentino, J. Non-Cryst. Solids **266-269**, 598 (2000).
[37] C. Piamonteze, A. C. Iñiguez, L. R. Tessler, M. C. Alves, and H. Toletino, Phys. Rev. Lett. **81**, 4652 (1998).
[38] V. F. Masterov, F. S. Nesredinov, P. P. Seregin, V. Kh. Kudoyarova, A. N. Kuznetsov, and E. I. Terukov, Appl. Phys. Lett. **72**, 728 (1998).
[39] D. L. Adler, D. C. Jacobson, D. J. Eaglesham, M. A. Marcus, J. L. Benton, J. M. Poate, and P. H. Citrin, Appl. Phys. Lett. **61**, 2181 (1992).
[40] L. R. Tessler and A. C. Iñiguez, J. Non-Cryst. Solids **266-269**, 603 (2000).
[41] E. I. Terukov, Y. K. Undalov, V. Kh. Kudoyarova, K. V. Koughia, J. P. Kleider, M. Gueunier, and R. Meaudre, J. Non-Cryst. Solids **299-302**, 699 (2002).
[42] C. Piamonteze, L. R. Tessler, H. Tolentino, M. do Carmo Martins Alves, G. Weiser, and E. I. Terukov, in *Amorphous and Heterogeneous Silicon Thin Films—2000*, edited by R. W. Collins, H. M. Branz, S. Guha, H. Okamoto, and M. Stutzmann, MRS Symposia Proceedings No. 609 (Pittsburgh, 2000), p. A11.2.1.
[43] H. Przybylinska, W. Jantsch, Yu. Suprun-Belevitch, M. Stepikhova, L. Palmetshofer, G. Hendorfer, R. J. Wilson, and B. J. Sealy, Phys. Rev. B **54**, 2532 (1996).
[44] N. Q. Vinh, H. Przybylinska, Z. F. Krasilnik, and T. Gregorkiewicz, Phys. Rev. Lett. **90**, 066401 (2003).
[45] W. Fuhs, I. Ulber, G. Weiser, M. S. Bressler, O. B. Gusev, A. M. Kuznetsov, V. Kh. Kudoyarova, E. I. Terukov, and I. N. Yassievich, Phys. Rev. B **56**, 9545 (1997).
[46] R. A. Street and J. C. Knights, Philos. Mag. B **42**, 551 (1980).
[47] W. B. Jackson and R. J. Nemanich, J. Non-Cryst. Solids **59-60**, 353 (1983).
[48] A. M. Glass, Phys. Today **46** (10), 34 (1993).
[49] E. Desurvire, Phys. Today **47** (1), 20 (1994).
[50] J. L. Zyskind, C. R. Giles, J. R. Simpson, and D. J. DiGiovanni, Design&Elektronik **23**, 59 (1993).
[51] M. Fujii, M. Yoshida, Y. Kanzawa, S. Hayashi, and K. Yamamoto, Appl. Phys. Lett. **71**, 1198 (1997).
[52] M. Fujii, M. Yoshida, S. Hayashi, and K. Yamamoto, Appl. Phys. Lett. **84**, 4525 (1998).
[53] K. Watanabe, M. Fujii, and S. Hayashi, in *Proceedings of the 25th International Conference on the Physics of Semiconductors Osaka, 2000*, edited by N. Miura and T. Ando, Springer Proceedings in Physics No. 87 (Springer, Berlin, 2001), p. 1177.
[54] U. Fano, Phys. Rev. **124**, 1866 (1961).
[55] A. Polman, J. Appl. Phys. **82**, 1 (1997).
[56] F. Priolo, G. Franzò, S. Coffa, S. Libertino, R. Barklie, and D. Carey, J. Appl. Phys. **78**, 3874 (1995).
[57] F. Priolo, G. Franzò, S. Coffa, and A. Carnera, Phys. Rev. B **57**, 4443 (1998).
[58] M. Needels, M. Schlüter, and M. Lannoo, Phys. Rev. B **47**, 15 533 (1993).
[59] P. G. Kik, M. J. A. de Dood, K. Kikoin, and A. Polman, Appl. Phys. Lett. **70**, 1721 (1997).
[60] A. Taguchi, K. Takahei, M. Matsuoka, and S. Tohno, J. Appl. Phys. **84**, 4471 (1998).
[61] A. J. Neuhalfen and B. W. Wessels, Appl. Phys. Lett. **60**, 2657 (1992).
[62] T. Benyattou, D. Seghier, G. Guillot, R. Moncorge, P. Galtier, and M. N. Charasse, Appl. Phys. Lett. **58**, 2132 (1991).
[63] J. Heber, J. Neukum, M. Altwein, R. Demirbilek, and N. Bodenschatz, Spectrochim. Acta, Part A **54**, 1557 (1998).
[64] S. G. Bishop, D. A. Turnbull, and B. G. Aitken, J. Non-Cryst. Solids **266-269**, 876 (2000).
[65] S. B. Aldabergenova, M. Albrecht, A. A. Andreev, C. Inglefield, J. Viner, V. Yu. Davydov, P. C. Taylor, and H. P. Strunk, J. Non-Cryst. Solids **283**, 173 (2001).
[66] I. N. Yassievich, M. S. Bresler, and O. B. Gusev, J. Phys.: Condens. Matter **9**, 9415 (1997).
[67] Th. Förster, Discuss. Faraday Soc. **27**, 7 (1954).

[68] Th. Förster, Z. Elektrochem. **64**, 157 (1960).
[69] D. L. Dexter, J. Chem. Phys. **21**, 836 (1953).
[70] D. M. Basko, G. C. La Rocca, F. Bassani, and V. M. Agranovich, Eur. Phys. J. B **8**, 353 (1999).
[71] D. M. Basko, V. M. Agranovich, G. Bassani, and G. C. La Rocca, Eur. Phys. J. B **13**, 653 (2000).
[72] C. Delerue and M. Lanoo, Phys. Rev. Lett. **67**, 3006 (1991).
[73] I. N. Yassievich and L. C. Kimerling, Semicond. Sci. Technol. **8**, 718 (1993).
[74] J. Michel, L. V. C. Assali, M. T. Morse, and L. C. Kimerling, Semicond. Semimetals **49**, 111 (1998).
[75] J. Wan, Y. Ling, Q. Sun, X. Wang, Phys. Rev. B **58**, 10 415 (1998).
[76] C. Piamonteze, L. R. Tessler, H. Tolentino, M. do Carmo Martins Alves, G. Weiser, and E. I. Terukov, in *Amorphous and Heterogeneous Silicon Thin Films—2000*, edited by R. W. Collins, H. M. Branz, S. Guha, H. Okamoto, and M. Stutzmann, MRS Symposia Proceedings No. 609 (Pittsburgh, 2000), p. A11.1.1.
[77] A. Janotta, Y. Dikce, M. Schmidt, Chr. Eisele, M. Luysberg, L. Houben, and M. Stutzmann, J. Appl. Phys. (unpublished).
[78] Sample provided by E. I. Terukov, Ioffe Institute, St. Petersburg, Russia.